

Editor Initial Decision: Reconsider after major revisions (02 Sep 2015)

By Prof. Wolfgang Wagner

Thank you very much for your responses. I am quite satisfied by them but, nonetheless, I would like to invite the two reviewers to comment the revised version as well. Therefore please submit your revised paper taking two additional comments into account:

We appreciate the editor's feedback and decision to reconsider our updated manuscript. We make some revision based on the editor's comments and have uploaded our revised manuscript. Responses to the specific comments are provided below (editor's comments are marked in blue italic font and our replies in black). Line numbers are marked according to the revised paper without tracked changes if not specified.

1) You write that "Unfortunately the lowest microwave frequency of AMSR2 precludes retrieving soil moisture from many areas with heavy vegetation". Please note that the performance of SMOS over really dense vegetation is not much better than for AMSR-E, reflecting the fact that neither C nor L-band can penetrate dense forests and shrubs.

We agree with the editor and acknowledge that SMOS, AMSR-E and AMSR2 have relatively similar performances over densely vegetated areas. We would like to address that while SMOS, AMSR-E and AMSR2 have shown to some limitations, the latest SMAP results are promising. Over densely vegetated areas, SMAP seems to outperform SMOS (both L-band) and the earlier C-band missions. Additionally, SMAP provides information on deeper soil moisture layers compared to the AMSR-E and AMSR2 retrievals. This could reduce the impact of the soil moisture saturation problem and hence improve the potential for satellite precipitation correction. However, information on the land surface temperatures remains unavailable for SMAP. Therefore, in this paper we focus on improving precipitation relying solely on soil moisture products. This has been revised and further clarified in line 87-93 (line 117-122 with tracked changes).

2) You use 1:30PM retrievals which is really unusual for passive microwave studies. Have you made comparisons to the AM retrievals? Does the LSMEM retrieval not assume that soil and vegetation temperature is the same?

First of all we would like to thank the editor for this comment. We agree that the descending (1:30AM) is better than the ascending (1:30PM) overpass. However, we believe expanding our study to include results from descending overpass would add little to the proof of concept and the focus of this paper. The results shown from 1:30PM retrievals (without 1:30AM retrievals) are able to show the potential impact of the improved data assimilation approach, and its impact on the reduction of errors in satellite precipitation retrievals. Further improvement in the correction of satellite precipitation could be expected when our methodology is used in combination with other (new) satellite soil moisture systems. The choice of SM products used is discussed in section 5 of the updated paper between line 532 and 536 (line 726-730 with tracked changes).

1 Correction of real-time satellite precipitation with 2 satellite soil moisture observations

3

4 Wang Zhan¹, Ming Pan¹, Niko [Wanders](#)^{1,2}, Eric F. Wood¹

5 [1] Department of Civil and Environmental Engineering, Princeton University, Princeton,
6 NJ, USA

7 [2] Department of Physical Geography, Utrecht University, Utrecht, the Netherland

8

9 Abstract

10 Rainfall and soil moisture are two key elements in modeling the interactions between the
11 land surface and the atmosphere. Accurate and high-resolution real-time precipitation is
12 crucial for monitoring and predicting the on-set of floods, and allows for alert and
13 warning before the impact becomes a disaster. Assimilation of remote sensing data into a
14 flood-forecasting model has the potential to improve monitoring accuracy. Space-borne
15 microwave observations are especially interesting because of their sensitivity to surface
16 soil moisture and its change. In this study, we assimilate satellite soil moisture retrievals
17 using the Variable Infiltration Capacity (VIC) land surface model, and a dynamic
18 assimilation technique, a particle filter, to adjust the Tropical Rainfall Measuring Mission
19 Multi-satellite Precipitation Analysis (TMPA) real-time precipitation estimates. We
20 compare updated precipitation with real-time precipitation before and after adjustment
21 and with NLDAS gauge-radar observations. Results show that satellite soil moisture
22 retrievals provide additional information by correcting errors in rainfall bias. [The](#)
23 [assimilation is](#) most effective in the correction of [medium](#) rainfall under dry to normal
24 surface condition; while limited/negative improvement is seen over wet/saturated
25 surfaces. [On the other hand, high frequency noises in satellite soil moisture impact the](#)
26 [assimilation by increasing rainfall frequency. The noise causes larger uncertainty in the](#)

Authors 8/31/2015 3:38 PM

Deleted: Wanders²

Authors 8/31/2015 3:38 PM

Deleted: High accuracy soil moisture retrievals, when merged with precipitation, generally increase both rainfall frequency and intensity, and are

Authors 8/31/2015 3:38 PM

Deleted: Errors from soil moisture, mixed among

Authors 8/31/2015 3:38 PM

Deleted: real signal, may generate a

35 | false-alarmed rainfall over wet regions. A threshold of 2 mm/day soil moisture change is
36 | identified and applied to the assimilation, which masked out most of the noise.

Authors 8/31/2015 3:38 PM

Deleted: signal approximately 2mm

Authors 8/31/2015 3:38 PM

Deleted: and thus lower the precipitation accuracy after adjustment.

37
38

39 | **1 Introduction**

40 | Precipitation is perhaps the most important variable in controlling energy and mass fluxes
41 | that dominate climate and particularly the terrestrial hydrological and ecological systems.
42 | Precipitation estimates, together with hydrologic models, provide the foundation for
43 | understanding the global energy and water cycles (Sorooshian, 2004; Ebert et al., 2007).
44 | However, obtaining accurate measurements of precipitation at regional to global scales
45 | has always been challenging due to its small-scale, space-time variability, and the sparse
46 | networks in many regions. Such limitations impede precise modeling of the hydrologic
47 | responses to precipitation. There is a clear need for improved, spatially distributed
48 | precipitation estimates to support hydrological modeling applications.

49 | In recent years, remotely sensed satellite precipitation has become a critical data source
50 | for a variety of hydrological applications, especially in poorly monitored regions such as
51 | sub-Saharan Africa due to its large spatial coverage. To date, a number of fine-scale,
52 | satellite-based precipitation estimates are now in operational production. One of the most
53 | frequently used is the Tropical Rainfall Measuring Mission Multi-satellite Precipitation
54 | Analysis (TMPA) product (Huffman et al., 2007). Over the 17 years lifetime since the
55 | launch of the Tropical Rainfall Measuring Mission (TRMM) in 1997, a series of high
56 | resolution (0.25-degree and 3-hourly), quasi-global (50°S - 50°N), near-realtime,
57 | TRMM-based precipitation estimates have been developed and made available to the
58 | research and applications communities (Huffman et al., 2007; 2010). Flood forecasting
59 | and monitoring is one major application for real time satellite rainfall products (Wu et al,
60 | 2014). However, the applicability of satellite precipitation products for near real-time
61 | hydrological applications that include drought and flood monitoring has been hampered
62 | by their need for gauge-based adjustment.

66 While it is possible to create such estimates solely from one type of sensor, researchers
67 have increasingly moved to using combinations of sensors in an attempt to improve
68 accuracy, coverage and resolution. A promising avenue for rainfall correction is through
69 the assimilation of satellite-based surface soil moisture into a water balance model (Pan
70 and Wood, 2006). Over land, the physical relationship between variations in soil water
71 storage and rainfall accumulation contain complementary information that can be
72 exploited for the mutual benefit of both types of products (Massari et al., 2014; Crow et
73 al., 2009). Unlike instantaneous rain rate, satellite surface soil moisture retrievals utilize
74 low frequency microwave signals and possess some memory reflecting antecedent
75 rainfall amounts.

76 Studies have demonstrated that in situ (Brocca et al., 2009, 2013; Matgen et al., 2012)
77 and satellite (Francois et al., 2003; Pellarin et al., 2008, 2013; Brocca et al., 2014)
78 estimates of surface soil moisture could contribute to precipitation estimates by providing
79 useful information concerning the sign and magnitude of antecedent rainfall
80 accumulation errors. In particular, Brocca et al. (2014) estimated daily rainfall on a global
81 scale based on satellite SM products by inverting the soil water balance equation. Crow et
82 al. (2003, 2009, 2011) corrected space-borne rainfall retrievals by assimilating remotely
83 sensed surface soil moisture retrievals into an Antecedent Precipitation Index (API) based
84 soil water balance model using a Kalman filter (Kalman, 1960). However, these studies
85 focused on multi-day aggregation periods and a space aggregated correction at 1°
86 resolution for the corrected precipitation totals. This limits their applicability in
87 applications such as near real-time flood forecasting. Wanders et al. (2015) tried to
88 overcome this limitation by the correction of 3 hourly satellite precipitation totals with a
89 set of satellite soil moisture and land surface temperature observations. One important
90 conclusion by Wanders et al. (2015) is that their results showed the limited potential for
91 satellite soil moisture observations for correcting precipitation if “all-weather” – i.e.
92 microwave based – land surface temperatures are available coincidently and at high
93 spatial resolution as was the case with AMSR-E.

94 But this isn't always the case, and it is also noted that current low-frequency microwave
95 soil moisture missions (specifically SMAP and SMOS) don't have radiometers at

Authors 8/31/2015 3:38 PM

Deleted: spaceborne

Authors 8/31/2015 3:38 PM

Deleted: a simple

Authors 8/31/2015 3:38 PM

Deleted: The hydrologic response

Authors 8/31/2015 3:38 PM

Deleted: to precipitation is especially

Authors 8/31/2015 3:38 PM

Deleted: in

Authors 8/31/2015 3:38 PM

Deleted: an explicit and sophisticated physical model is needed to accurately recover

Authors 8/31/2015 3:38 PM

Deleted: information about the rainfall more precisely, e.g. wetted area. This is because most storm systems have a very strong and complicated spatial structure that is non-Gaussian and non-stationary in both time and space (Wanders et al., 2015).

Authors 8/31/2015 3:38 PM

Deleted: In this paper we present a method to improve real-time remote sensing precipitation products by merging retrievals with soil moisture remote sensing products through a Particle Filter (PF),

114 [frequencies useful for estimating land surface temperatures, even though a 37 GHz sensor](#)
115 [is part of the AMSR2 system. In fact SMAP and ECMWF/SMOS use LST from weather](#)
116 [models analysis fields in their algorithms. Unfortunately the lowest microwave frequency](#)
117 [of AMSR2 and SMOS precludes retrieving soil moisture from many areas with heavy](#)
118 [vegetation, and AMSR2 has a significant dry bias with less availability than AMSR-E,](#)
119 [but is no longer operable. So improvements to satellite precipitation from the Global](#)
120 [Precipitation Mission products must rely solely on satellite soil moisture products from](#)
121 [SMAP, which is promises better soil moisture retrievals due to increased penetration](#)
122 [depth, and the improvements to the assimilation algorithms is the goal of this study.](#)

123 [Thus, we focus exclusively on the usefulness of assimilating soil moisture products to](#)
124 [improve satellite rainfall. We propose as part of the work how to improve the generation](#)
125 [of rain particles and the bias-correction of the satellite soil moisture observations, as well](#)
126 [as to enhance the assimilation algorithm to maximize the information that can be gained](#)
127 [from using soil moisture alone to adjust precipitation. Due to the very strong and](#)
128 [complicated spatial structure of precipitation, that is non-Gaussian and non-stationary in](#)
129 [both time and space \(Wanders et al., 2015\), a more advanced method is applied to](#)
130 [generate possible precipitation fields than were used in earlier studies or in Wanders et al.](#)
131 [2015\) \(see section 2.2.2\). Furthermore, a more advanced bias correction method is also](#)
132 [applied to account for the reported problems in the second order statistics of the soil](#)
133 [moisture retrievals. We used a soil moisture remote sensing product to improve real-time](#)
134 [remote sensing precipitation product, TMPA 3B42RT, through a Particle Filter \(PF\) and](#)
135 [therefore offer an improved basis for quantitatively monitoring and predicting flood](#)
136 [events, especially in those parts of the world where in-situ networks are too sparse to](#)
137 [support more traditional methods of hydrologic monitoring and prediction. The](#)
138 [precipitation enhancement experiments are carried out over the continental U.S.](#)
139 [\(CONUS\) and the precipitation skill is validated against the NLDAS gauge-radar](#)
140 [precipitation product. Section 5 presents a comparison of the results from this study to](#)
141 [the earlier studies related to improving satellite precipitation.](#)

Wang Zhan 9/3/2015 11:13 PM

Deleted:

Wang Zhan 9/3/2015 11:48 PM

Deleted: data availability of

Wang Zhan 9/3/2015 11:48 PM

Deleted: is

Wang Zhan 9/3/2015 11:48 PM

Deleted: significantly less than

Wang Zhan 9/4/2015 12:01 AM

Deleted: and SMOS

Wang Zhan 9/4/2015 12:11 AM

Deleted:

148 **2 Methods**

149 **2.1 Overview**

150 Random replicates of satellite precipitation are generated based on real-time TMPA
151 (3B42RT) retrievals and its uncertainty (Pan et al., 2010), which are then used to force
152 the VIC land surface model (LSM) where one output of interest is surface soil moisture.
153 Satellite soil moisture data products are compared and merged with the 3B42RT product
154 to improve the accuracy of the satellite precipitation estimates. A schematic for the study
155 approach is provided in Figure 1. Based on real-time 3B42RT retrievals, a set of possible
156 precipitation estimates (a.k.a. replicates or particles) $\{p^i\}_{i=1,2,\dots,N}$ is generated with
157 assigned initial prior probability weights $\{w^i\}_{i=1,2,\dots,N}$. These rainfall rates are then used
158 to force the VIC land surface model to produce soil moisture predictions $\{\theta^i\}_{i=1,2,\dots,N}$.
159 Retrievals of AMSR-E satellite surface soil moisture using the Land Surface Microwave
160 Model (LSMEM) (Pan et al., 2014) are then merged with the LSM-based soil moisture
161 within the Particle Filter (PF) that compares AMSR-E/LSMEM changes in soil moisture,
162 ΔSM , to the LSM predicted soil moisture changes. From these, posterior weights
163 $\{w^{i+}\}_{i=1,2,\dots,N}$ are calculated for each precipitation member (particle) that takes into
164 account the uncertainties of AMSR-E/LSMEM ΔSM retrievals. From these updated
165 weights, an updated precipitation probability distribution is constructed, where the
166 precipitation particle with highest probability is taken as the “best” adjusted precipitation
167 estimate ($3B42RT_{ADJ}$). The procedure is carried out over the continental US (CONUS)
168 region on a grid-by-grid basis (0.25-degree) and a daily time step. Allowing for 6 months
169 model spin-up period, the adjustment is done from January 2003 to July 2007.

170 **2.2 Modeling, Statistical Tools and Data Sources**

171 **2.2.1 The Particle Filter**

172 Data assimilation methods are capable of dynamically merging predictions from a state
173 equation (i.e. the land surface model) with measurements (i.e. AMSR-E retrievals) to
174 minimize uncertainties from both the predictions and measurements. It is assumed that

175 the source of uncertainty in the land surface model predictions come solely from the real-
 176 time satellite precipitation, so that the particle filter (PF) provides an algorithm to update
 177 the precipitation based on the AMSR-E retrievals. The state evolution of a particle filter
 178 from discrete time $t-1$ to t can be represented as:

$$179 \quad \theta_t = f_t(\theta_{t-1}, p_t, \kappa_t, \alpha_t) \quad (1)$$

180 where θ_t is the 1st layer soil moisture at time t , whose value is predicted by the state
 181 equation Eq.(1) as $f_t(\bullet)$, and in the study is the hydrological model VIC, which takes in
 182 forcing data, including precipitation (p_t) and other forcings (κ_t); and simulates land
 183 surface states (soil moisture and soil temperatures at various levels, snow, etc.) and fluxes
 184 (evapotranspiration, runoff) at time t . Herein we are basically interested only in the 1st
 185 layer (top 10cm) soil moisture state and precipitation forcing, so other states and fluxes
 186 are not explicitly shown. α_t is the random error in the prediction of θ_t , whose statistics
 187 are known but not its value at any specific time.

188 At time t , the satellite surface soil moisture retrieval, θ_t^* , can be related to the VIC
 189 modeled 1st layer soil moisture θ_t as:

$$190 \quad \theta_t^* = h_t(\theta_t, \beta_t) \quad (2)$$

191 where h_t is taken as a regression that transforms the VIC simulated 1st layer soil
 192 moisture to satellite surface soil moisture. β_t is the noise in this regression relationship.
 193 The two noises α_t and β_t are assumed to be independent of each other at all times t .

194 At time t , given a 3B42RT precipitation estimate, p_t^{sat} , a set of N precipitation replicates
 195 $\{p_t^i\}_{i=1,2,\dots,N}$ and their associated initial prior probability weight $\{w_t^i\}_{i=1,2,\dots,N}$ are
 196 generated.

$$197 \quad g(p_t^{\text{sat}}) \sim \{p_t^i, w_t^i\}_{i=1,2,\dots,N} \quad (3)$$

$$198 \quad \sum_{i=1}^N w_t^i = 1 \quad (4)$$

199 $g(\cdot)$ is a probability density function. For N precipitation replicates, $\{p_t^i\}_{i=1,2,\dots,N}$, the
 200 propagation of the states from time step $(t-1)$ to t is by the VIC land surface model

201 represented in Eq.(1). The VIC land surface model simulates the 10cm 1st layer soil
202 moisture, $\{\theta_t^i\}_{i=1,2,\dots,N}$ for each precipitation replicate.

$$203 \quad \{\theta_t^i = f_t(\theta_{t-1}, p_t^i, \kappa_t, \alpha_t)\}_{i=1,2,\dots,N} \quad (5)$$

204 with the associated weights assigned to the precipitation member:

$$205 \quad \{\theta_t^i, w_t^i\}_{i=1,2,\dots,N} = \{f_t(\theta_{t-1}, p_t^i, \kappa_t, \alpha_t), w_t^i\}_{i=1,2,\dots,N} \quad (6)$$

206 If the satellite soil moisture retrieval at time t is θ_t^* , the update of precipitation forcing is
207 accomplished by updating the importance weight of each replicate given the
208 “measurement” θ_t^* :

$$209 \quad w_t^{i+} \sim \{g(\theta_t^i | \theta_t^*)\}_{i=1,2,\dots,N} \quad (7)$$

$$210 \quad \sum_{i=1}^N w_t^{i+} = 1 \quad (8)$$

211 The likelihood function $g(\theta_t^i | \theta_t^*)$ can be derived from h_t and $g(\beta_t)$. The schematic of the
212 utilized strategy is shown in [Figure 2](#). The primary disadvantage of the particle filter is
213 the large number of replicates required to accurately represent the conditional probability
214 densities of p_t and θ_t . When the measurements exceed a few hundred, the particle filter is
215 not computationally practical for land surface problems. Considering computation
216 efficiency, we set the number of independent particles, N, from the prior distribution to
217 be 200.

218 **2.2.2 Precipitation Replicates Generation**

219 We generate precipitation replicates, $\{p_t^i\}_{i=1,2,\dots,N}$, based on statistics comparing NLDAS

220 and 3B42RT precipitation, as shown in [Figure 3](#). Given a 3B42RT precipitation

221 measurement (binned by magnitude), with bin minimum and maximum indicated in

222 [Figure 3](#), precipitation replicates are generated based on the corresponding 15th, 30th, 70th,

223 85th percentiles and the maximum NLDAS precipitation of the particular quantile bin as

224 follows: 15% of the replicates are generated with values uniformly distributed from 0 and

225 15th percentile; 15% of replicates with values from 15th to 30th percentile; 20% of

226 replicates with values from 30th percentile to the median; 20% of the replicates generated

227 from the median to 70th ; 15% with values from 70th to 85th percentile; and 15% from the

Wang Zhan 9/7/2015 10:49 PM

Deleted: Figure 2

Wang Zhan 9/7/2015 10:49 PM

Deleted: Figure 3

Wang Zhan 9/7/2015 10:49 PM

Deleted: Figure 3

231 85th percentile to the maximum precipitation value. Note that although the generation of
232 particles is based on statistics calculated from NLDAS, results show little difference
233 generating precipitation ensembles uniformly distributed between 0 and 200 mm/day.

234 **2.2.3 AMSR-E/LSMEM Soil Moisture Retrievals**

235 The soil moisture product is derived from multiple microwave channels of the Advanced
236 Microwave Scanning Radiometer for EOS (AMSR-E) instrument. The retrieval algorithm
237 by Pan et al. (2014) is an enhanced version of the Land Surface Microwave Emission
238 Model (LSMEM). The near surface soil moisture and vegetation optical depth (VOD) are
239 estimated simultaneously from a dual polarization approach that utilizes both horizontal
240 (H) and vertical (V) polarizations measurement by the space-borne sensor. The input
241 AMSR-E brightness temperature comes from the NSIDC AMSR-E/Aqua Daily Global
242 Quarter-Degree Gridded Brightness Temperatures product (overlapping swaths in the
243 same day are truncated so that only the latest one is present). Consequently, the soil
244 moisture retrievals are also gridded at 0.25-degree with one ascending map and one
245 descending map at the daily time step. A maximum threshold value of $0.6 \text{ m}^3/\text{m}^3$ has been
246 applied manually to reduce error from open water bodies. According to Pan et al. (2014),
247 the soil moisture dataset based on observations from AMSR-E are shown to be consistent
248 at large scales in terms of reproducing the spatial pattern of soil moisture from VIC land
249 surface model simulation. Ascending soil moisture retrievals (equatorial crossing time
250 1:30PM local time) is assimilated in this study.

251 Similarly, while the spatial patterns of the basic statistics of AMSR-E/LSMEM SM
252 retrievals compare well to VIC simulations (Pan et al., 2014), VIC has its top layer (10
253 cm), which is deeper than the detection depth of AMSR-E, so that the mean and temporal
254 variability of the retrievals are higher than the VIC simulated soil moisture (Figure 4 in
255 Pan et al., 2014). Considering this difference between detection depths, we pre-process
256 soil moisture retrievals as follows:

257 1) Rescale soil moisture retrievals (AMSR-E/LSMEM SM) to have the same minimum
258 and maximum range as VIC simulated 1st layer soil moisture.

260 2) Calculate a daily soil moisture change. As satellite retrievals are manually truncated to
261 be no more than $0.6 \text{ m}^3/\text{m}^3$ (equivalent to 60mm of water in the top soil layer in VIC),
262 retrievals larger than $0.6 \text{ m}^3/\text{m}^3$ are excluded.

263 3) Fit a 2nd order polynomial regression model with ΔSM (all units in mm of water in the
264 top layer) from satellite and VIC simulation on a monthly basis and 3×3 grid scale
265 (window).

266 After pre-processing, the distribution of soil moisture change matches fairly well with
267 $\Delta\text{SM}_{\text{VIC}}$ (Figure 4). The mean absolute difference reduces from a spatial average of 5.25
268 mm/day to 0.71 mm/day, with relatively larger value over eastern CONUS. According to
269 Pan et al. (2014), the no-skill or negative-skill areas occur mostly over eastern dense
270 forests due to vegetation blockage of the soil moisture signal (Pan et al., 2014). The
271 accuracy of soil moisture retrievals is also limited by mountainous topography and the
272 occurrence of snow and frozen ground during winter whose identification from satellite
273 observations is often difficult. For the purpose of this study, we assign zero weight to the
274 $3\text{B42RT}_{\text{ADJ}}$ and rely exclusively on the initial 3B42RT precipitation for time steps when
275 the VIC model predicts snow cover or frozen surfaces.

276 **2.2.4 VIC Land Surface Model**

277 The Variable Infiltration Capacity (VIC) model (Liang et al., 1994; Gao et al., 2010) is
278 used to dynamically simulate the hydrological responses of soil moisture to precipitation,
279 surface radiation and surface meteorology. The VIC model solves the full energy and
280 water balance over each 0.25-degree-grid-cell independently, thus ensuring its
281 computational efficiency. The assumption of independency poses limitation on the
282 application of LSM at very high spatial resolution (e.g. $1\text{km}\times 1\text{km}$) over large areas.
283 Three-layer-soil-moisture is simulated through a soil-vegetation-atmosphere transfer
284 (SVAT) scheme, which also accounts for sub-grid scale heterogeneity of vegetation, soil
285 and topography. A detailed soil moisture algorithm description can be found in Liang et
286 al. (1996). The VIC model has been validated extensively over CONUS by evaluating
287 soil moisture and simulations to observations (Robock et al., 2003; Schaake et al., 2004).

Wang Zhan 9/7/2015 10:49 PM

Deleted: Figure 4

289 **3 Idealized Experiment**

290 Before applying the Particle Filter assimilation algorithm on 3B42RT precipitation
291 estimates, we conducted an idealized experiment where we treat the NLDAS
292 precipitation as the “truth” and the NLDAS precipitation forced VIC simulations as
293 “satellite observed” soil moisture. As an idealized experiment, we adjust TMPA real-time
294 precipitation estimates based on these “satellite observations”. Phase 2 of the North
295 American Land Data Assimilation System (NLDAS-2) rainfall forcing combines hourly
296 WSR-88D radar analyses from the National Weather Service (NWS) and daily gauge
297 reports (~13,000/day) from the Climate Prediction Center (CPC) (Ek et al., 2011). The
298 dataset, with a spatial resolution of 0.125 degree and hourly observations, was pre-
299 processed into 0.25-degree daily precipitation to be consistent with that of 3B42RT and
300 AMSR-E/LSMEM SM datasets. Hourly NLDAS and 3-hourly 3B42RT precipitation is
301 aggregated into daily precipitation defined by a period shifted ~7.5 hours into the future
302 (9:00PM-9:00PM), allowing for a necessary delay for soil moisture to respond to
303 incoming rainfall. The idealized experiment is designed to test whether the algorithm is
304 able to retrieve rainfall forcing with soil moisture change, assuming that the soil moisture
305 observations are 100% accurate.

306 Results show that, with the knowledge of 1st layer soil moisture change (via the “satellite
307 observations”), the adjustment is able to recover intensity and spatial pattern of forcing
308 precipitation (Figure 5g). Average mean absolute error (MAE) of daily rainfall amount is
309 reduced by 52.9% (2.91 mm/day to 1.37 mm/day) over the region. Figure 5a to Figure 5e
310 shows an example of the recovered rainfall field from the idealized experiment for 27th
311 Oct. 2003. The spatial pattern matches the original NLDAS precipitation well.

312 **3.1 Effect of surface soil saturation**

313 While successfully recovering the general pattern of NLDAS precipitation based on first
314 layer soil moisture, the idealized experiment is not always able to recover the
315 precipitation volume due to the fact that the top layer soil moisture alone does not contain
316 the complete memory of the previous day’s rainfall. Deeper soil moisture,
317 evapotranspiration and runoff also carry part of this information. As the surface gets

Authors 8/31/2015 3:38 PM
Deleted: Figure 6.

Wang Zhan 9/7/2015 10:49 PM
Deleted: Figure 5

Authors 8/31/2015 3:38 PM
Deleted: 91mm

Authors 8/31/2015 3:38 PM
Deleted: 37mm

Wang Zhan 9/7/2015 10:49 PM
Deleted: Figure 5

Wang Zhan 9/7/2015 10:49 PM
Deleted: Figure 5

324 wetter, the VIC 1st layer soil moisture has smaller variation. If the incoming precipitation
325 brings the surface to saturation, the VIC model redistributes the soil moisture vertically
326 through vertical moisture flow and generates runoff. Hence soil moisture increments,
327 ΔSM , near saturation are less correlated with incoming precipitation as they change
328 minimally to additional incoming rainfall. An example demonstrating this saturation
329 effect is shown in [Figure 5f](#) to [Figure 5j](#). When incoming precipitation brings the surface
330 SM to (near) saturation, there is very limited improvement after the adjustment. Because
331 of the low sensitivity of the soil surface to precipitation, there is little change in ΔSM in
332 response to precipitation variations among the replicates. It is almost always the case that
333 the algorithm is not able to find a “matching” ΔSM .

334 We separately evaluate the skill improvement in the recovered NLDAS precipitation with
335 and without surface saturation. [Figure 6](#) confirms the effect of surface saturation on
336 [adjusted precipitation, which is well described in previous studies \(e.g. Brocca et al.,
337 \[2013, 2014\]\(#\)\)](#). The recovered precipitation, when the surface soil is saturated, only
338 contributes more noise rather than an improvement to the rainfall estimates. The VIC
339 model computes the moisture flow between soil layers using an hourly time step. If the 1st
340 layer soil moisture exceeds its maximum capacity, it is considered to be a surface
341 saturation case. As seen in [Figure 5](#), there is very limited or negative skill in the
342 recovered precipitation under saturated surface soil moisture conditions. Such
343 circumstances are identified and the AMSR-E/LSMEM ΔSM observation disregarded by
344 assigning zero weight to the $3B42RT_{ADJ}$ values. Thus for wetter areas with heavy
345 precipitation that potentially would bring the surface soil moisture to saturation, the
346 $3B42RT$ product is less likely to be adjusted according to satellite ΔSM and the best
347 precipitation estimate is $3B42RT$.

348 3.2 Effect of SM uncertainty

349 In the idealized experiment, NLDAS-VIC soil moisture is taken as truth with zero
350 uncertainty associated with (θ_t^*). However, this assumption is not valid for real satellite
351 SM retrievals, mean absolute error of which is approximately 3% vol./vol. (McCabe et
352 al., 2005). To consider this, we added error to the “truth” SM (normally distributed with
353 [zero mean and standard deviations of 1mm, 2mm, 3mm, 4mm and 5mm](#)), and simulated

Wang Zhan 9/7/2015 10:49 PM

Deleted: Figure 5

Wang Zhan 9/7/2015 10:49 PM

Deleted: Figure 5

Authors 8/31/2015 3:38 PM

Moved (insertion) [1]

Wang Zhan 9/7/2015 10:49 PM

Deleted: Figure 6

Authors 8/31/2015 3:38 PM

Deleted: (Figure 6).

Wang Zhan 9/7/2015 10:49 PM

Deleted: Figure 5

Authors 8/31/2015 3:38 PM

Deleted: 0.

Authors 8/31/2015 3:38 PM

Deleted: , 1.0mm, 1.5mm, 2.0mm, 2.5mm,
3.0mm, 3.5mm, 4.0mm 4.5mm and 5.0mm

362 | the effect of SM uncertainty to evaluate the associated adjustment errors. [Figure 7](#), shows
363 | that larger soil moisture observation errors lead to larger error variation after adjustment.
364 | This also suggests that soil moisture responds to precipitation non-linearly based on
365 | different initial conditions. An estimated wetter surface has lower sensitivity to an
366 | incoming rainfall amount, resulting in larger error in the recovered NLDAS precipitation.
367 | As shown in [Figure 7](#), the error standard deviation of the recovered NLDAS precipitation
368 | increases with surface water content (statistics shown in [Table 2](#)). As we add noise larger
369 | than $N(0, 1\text{mm})$ into “true” SM observation, there is a wet bias of approximately 1
370 | mm/day regardless of 1st layer soil moisture level. This suggests that when the difference
371 | between 1st layer SM and saturation is less than 8 mm , the median of the errors in the
372 | recovered NLDAS precipitation grows from 0.16 mm/day to 1.89 mm/day when we add
373 | $N(0, 5\text{mm})$ noise, while inter-quantile range (IQR) increases from 1.71 mm/day to 7.04
374 | mm/day . Acknowledging such a wet bias, to avoid introducing any more unintentional
375 | bias in the $3B42RT_{ADJ}$ estimates, we take as zero the uncertainty of AMSR-E/LSMEM
376 | SM retrievals, i.e. we take $h_t(\theta_t)$ as our single observation θ_t^* and adjust the $3B42RT$
377 | estimates accordingly.

378 | It is noteworthy that the soil moisture change is calculated based on previous days’ soil
379 | water contents. Therefore errors tend to accumulate over time until they are “re-set” when
380 | a significant precipitation event takes place. This type of uncertainty accounts for a small
381 | portion of the total error in the adjusted precipitation (black being the no error case in
382 | [Figure 7](#), with the “true” change in soil moisture from every time step). As complete
383 | global coverage is not provided with each orbit of the AMSR-E sensor, on average 44.01%
384 | of the time steps ($<0.6\text{ m}^3/\text{m}^3$) during the study period have observations, with more
385 | frequent overpasses at higher latitudes (Figure 4e in Pan et al., 2014). This observation
386 | gap unavoidably introduces extra uncertainty in the retrieval of the precipitation signal.
387 | To further avoid possible additional errors, we update the forcing rainfall when a ΔSM
388 | temporal match ($\pm 0.4\text{mm}$) is available, and keep the original precipitation if a match isn’t
389 | available.

Wang Zhan 9/7/2015 10:49 PM

Deleted: Figure 7

Wang Zhan 9/7/2015 10:49 PM

Deleted: Figure 7

Wang Zhan 9/7/2015 10:49 PM

Deleted: Table 2

Authors 8/31/2015 3:38 PM

Deleted: 0.5mm

Authors 8/31/2015 3:38 PM

Deleted: 1mm

Authors 8/31/2015 3:38 PM

Deleted: 8mm

Authors 8/31/2015 3:38 PM

Deleted: 16mm

Authors 8/31/2015 3:38 PM

Deleted: 89mm

Authors 8/31/2015 3:38 PM

Deleted: 5.0mm

Authors 8/31/2015 3:38 PM

Deleted: 71mm

Authors 8/31/2015 3:38 PM

Deleted: 04mm

Wang Zhan 9/7/2015 10:49 PM

Deleted: Figure 7

402 4 Improvement on real-time precipitation estimates and their validation

403 The adjustment of real TMPA 3B42RT retrievals based on AMSR-E/LSMEM Δ SM is
404 carried out using the methods described in Section 2.2.3, and results from the idealized
405 experiment (Sect. 3) with regard to the circumstances where an adjustment is applied.

406 An example of TMPA 3B42RT adjustment is provide in Figure 8, where a snapshot of
407 the rainfall field is shown (Figure 8b) and compared with NLDAS on May 26th 2006 and
408 the adjusted rainfall pattern based on AMSR-E/LSMEM Δ SM. The 3B42RT_{ADJ} rainfall
409 field (Figure 8c) is similar in terms of its spatial distribution compared to NLDAS
410 precipitation estimates (Figure 8d).

411 On average TMPA 3B42RT and AMSR-E/LSMEM Δ SM have a spatial Pearson
412 Correlation Coefficient of 0.37 (Shown in Figure 9, left), compared to 0.52 for the
413 correlation between NLDAS and Δ SM. After the adjustment procedure, the Pearson
414 correlation coefficient between 3B42RT_{ADJ} and AMSR-E/LSMEM Δ SM increases to
415 0.53, (shown in Figure 9), indicating that the correction method is successful. A below
416 average increase in correlation is found over the western mountainous region, the Great
417 Lakes region and eastern high vegetated and populated region. Additionally, the satellite
418 soil moisture suffers from snow/ice/standing water contamination, which affects the
419 potential for improved results after correction. The 3B42RT_{ADJ} has significant
420 improvement over 3B42RT in terms of long-term precipitation bias. The bias in 3B42RT
421 annual mean precipitation is reduced by 20.6%, from -9.32mm/month spatial average in
422 3B42RT to -7.40mm/month in 3B42RT_{ADJ} (shown in Figure 9, right). Frequency of rain
423 days generally increases significantly everywhere, (Figure 10). The NLDAS data (Figure
424 10, right) suggests an almost constant drizzling rainfall over parts of the western
425 mountainous area (Montana, Idaho, Wyoming and Colorado), while assimilating AMSR-
426 E/LSMEM Δ SM datasets does not have a signal of higher rainfall frequency, (Figure 10,
427 middle). This is possibly due to lower soil moisture variability in satellite retrievals over
428 the dry, mountainous areas and frequent presence of snow and ice (3B42RT is not
429 updated under such circumstances).

430 Figure 11, shows the assimilation results for the grids and days with soil moisture
431 observations, using the NLDAS precipitation as a reference. Overall, the method is

Authors 8/31/2015 3:38 PM
Deleted: Actual...he adjustment of th ... [1]

Authors 8/31/2015 3:38 PM
Deleted: Figure 8 shows

Wang Zhan 9/7/2015 10:49 PM
Deleted: Figure 8

Authors 8/31/2015 3:38 PM
Deleted: from the 3B42RT

Wang Zhan 9/7/2015 10:49 PM
Deleted: Figure 8

Authors 8/31/2015 3:38 PM
Deleted: product

Wang Zhan 9/7/2015 10:49 PM
Deleted: Figure 8

Wang Zhan 9/7/2015 10:49 PM
Deleted: Figure 8

Authors 8/31/2015 3:38 PM
Deleted: d).

Authors 8/31/2015 3:38 PM
Deleted: has...ave a spatial ... [2]

Wang Zhan 9/7/2015 10:49 PM
Deleted: Figure 10...). The NLDAS ... [3]

Authors 8/31/2015 3:38 PM
Deleted: .

Wang Zhan 9/7/2015 10:49 PM
Deleted: Figure 10

Authors 8/31/2015 3:38 PM
Deleted:). The excessive 3B42RT_{ADJ} rainfall events comes from the high-frequency noise in AMSR-E/LSMEM soil moisture retrievals identified by Pan et, al (2004) and Wanders et al. (2015)

Authors 8/31/2015 3:38 PM
Deleted: Figure 9 presents false alarm rate (FAR) and probability of detection (POD) of 3B42RT and 3B42RT_{ADJ}, using NLDAS as reference dataset. The rain event threshold is set to be 0.1mm/day and 2mm/day. Comparing Figure 9a) and b), most of the excessive rainfall is less than 2mm/day. For a 0.1mm/day threshold, both FAR and POD increases 3B42RT_{ADJ} except for the mountainous region. Whereas for a 2mm/day threshold, there is only slight increase in FAR, mostly in eastern U.S. The dramatic overestimation of rainy days is also absent when 2mm/day event threshold is applied. Consistent with other studies, spatially, larger improvement is found in central U.S. The area coincides with where higher AMSR-E/LSMEM Δ SM accuracy lies (non- ... [4]

Wang Zhan 9/7/2015 10:49 PM
Deleted: Figure 11

545 successful in correcting daily rainfall amount when 3B42RT overestimates precipitation,
546 $(3B42RT - NLDAS > 0)$. Mean standard deviation (STD) of $3B42RT_{ADJ} - NLDAS$ is
547 between 1 and 3 mm/day (statistics provided in Table 3). When 3B42RT underestimates
548 rainfall, $(3B42RT - NLDAS < 0)$, the assimilation has limited improvement on 3B42RT.
549 This is due to the effect of surface saturation. In terms of adding rainfall, there are two
550 scenarios when the effectiveness of the assimilation is limited.

551 1) The presence of wet conditions or (near) saturation. There is higher probability
552 bringing the surface to saturation (wetter condition) when the assimilation adds
553 rainfall into 3B42RT. However soil moisture increments are less sensitive to
554 incoming precipitation on wetter soil. Therefore, an error in ΔSM often translates into
555 $3B42RT_{ADJ}$ in a magnified manner.

556 2) The presence of very heavy precipitation, which typically brings the surface to
557 saturation, hence not results in an update of 3B42RT, is not updated. If, by a small
558 probability, the surface is wet (nearly saturated) but not completely saturated after a
559 heavy rainfall, the updated 3B42RT also suffers from large uncertainty (explained in
560 1) above).

561 The effect of the assimilation conditioned on 3B42RT rainfall amount is further evaluated,
562 by skill scores. Figure 12 presents probability of detection (POD) and false alarm rate
563 (FAR) in 3B42RT and $3B42RT_{ADJ}$, using NLDAS as the reference dataset. The rain event
564 threshold is set to be 0.1 mm/day and 2 mm/day. This is possibly due to lower soil
565 moisture variability in satellite retrievals over the dry, mountainous areas and frequent
566 presence of snow and ice (3B42RT is not updated under such circumstances). For a 0.1
567 mm/day threshold, both FAR and POD increases in $3B42RT_{ADJ}$ except for the
568 mountainous region. Whereas for a 2 mm/day threshold, there is only slight increase in
569 FAR in most of eastern U.S. region. The overestimation of rain days is also absent when
570 2 mm/day event threshold is applied which suggests that most of the excessive rainy days
571 have less than 2 mm/day rain amount. Consistent with other studies, spatially, larger
572 improvements are found in the central U.S. The area coincides where higher AMSR-
573 E/LSMEM ΔSM accuracy is found (non-mountainous regions with little urbanization and
574 light vegetation). Despite of the regional variability, these excessive rainy days are a

Authors 8/31/2015 3:38 PM
Deleted: .

Authors 8/31/2015 3:38 PM
Deleted: 3mm

Wang Zhan 9/7/2015 10:49 PM
Deleted: Table 3

Authors 8/31/2015 3:38 PM
Deleted: ,

Authors 8/31/2015 3:38 PM
Deleted: a ΔSM

Authors 8/31/2015 3:38 PM
Deleted: to

Authors 8/31/2015 3:38 PM
Deleted: near

Authors 8/31/2015 3:38 PM
Deleted: a

Authors 8/31/2015 3:38 PM
Deleted: Since the prior knowledge of overestimated precipitation is not always available, the

Authors 8/31/2015 3:38 PM
Deleted: .

587 [result of the high-frequency noise in AMSR-E/LSMEM soil moisture retrievals identified](#)
588 [by Pan et al \(2004\) and Wanders et al. \(2015\).](#)

589 The applied method is ineffective for light rainfall [\(< 2 mm\)](#), where the adjustment tends to
590 over-correct precipitation by adding excessive rainfall – [mostly the result of the high](#)
591 [frequency AMSR-E noise. MAE of light rainfall \(< 2 mm/day\) increased from 0.65](#)
592 [mm/day in 3B42RT to 0.99 mm/day in 3B42RT_{ADJ}.](#) On the other hand, [satellite soil](#)
593 [moisture assimilation is very effective in correcting satellite precipitation larger than 2](#)
594 [mm/day: MAE of medium to large rainfall \(≥ 2 mm/day\) decreased from 7.07 mm/day in](#)
595 [3B42RT to 6.55 mm/day in 3B42RT_{ADJ}.](#) The effect of [the](#) assimilation is different over
596 the western mountainous region, the north-to-south central U.S. band and the eastern U.S.

597 The western mountainous region has a dry climatology with more frequent rainfall in
598 small [amounts](#). The white noise [in ΔSM](#), negatively impacting 3B42RT_{ADJ}, is comparable
599 to the positive improvement brought by [actual](#) light rainfall signals in ΔSM. Therefore,
600 the assimilation of ΔSM has no significant impact [in these regions](#).

601 The north-to-south band over central U.S. experiences more medium [to large \(≥ 2,](#)
602 [mm/day\)](#) rainfall. In addition, the region is lightly vegetated (annual mean LAI <1) with
603 low elevation ([< 1500 m](#)), where soil moisture retrievals are of higher accuracy. Soil
604 moisture climatology is wetter [in](#) the west, causing larger [variations](#) in 3B42RT_{ADJ} error
605 from the white noise ΔSM (as discussed in Section 3.2). Despite of that, satellite soil
606 moisture is most effective correcting medium to large rainfall [under](#) normal surface
607 [conditions](#).

608 The decreased skill in 3B42RT_{ADJ} over eastern U.S. is primarily attributed to both
609 precipitation and soil moisture climatology, [a](#) wet climate with more medium to large
610 rainfall, neither of which is suitable for soil moisture assimilation.

611 In summary, the high-frequency noise in soil moisture product [causes](#) a major limitation.
612 The noise impacts adjusted precipitation by introducing false alarm [rain](#) days. It is
613 difficult to distinguish the noise and [retrieve the](#) true rainfall signals. A remedy [to prevent](#)
614 the excessive [rain](#) days is applying a cutoff ΔSM threshold when [rain](#) days are added, at
615 the expense of neglecting a part of the true rainfall signals. [Figure 13](#) shows the
616 [probability of added rainy days being consistent with NLDAS \(NLDAS > 0 mm/day\)](#)

Authors 8/31/2015 3:38 PM
Deleted: <2mm

Authors 8/31/2015 3:38 PM
Deleted: coming

Authors 8/31/2015 3:38 PM
Deleted: the high frequency AMSR-E noise.

Authors 8/31/2015 3:38 PM
Deleted: Satellite

Authors 8/31/2015 3:38 PM
Deleted: of larger than 2mm/day.

Authors 8/31/2015 3:38 PM
Deleted: amount. Skills are limited by the white noise in ΔSM.

Authors 8/31/2015 3:38 PM
Deleted: real

Authors 8/31/2015 3:38 PM
Deleted: (

Authors 8/31/2015 3:38 PM
Deleted: -20mm

Authors 8/31/2015 3:38 PM
Deleted: 1500m

Authors 8/31/2015 3:38 PM
Deleted: than

Authors 8/31/2015 3:38 PM
Deleted: variation

Authors 8/31/2015 3:38 PM
Deleted: with

Authors 8/31/2015 3:38 PM
Deleted: condition

Authors 8/31/2015 3:38 PM
Deleted: is

Authors 8/31/2015 3:38 PM
Deleted: rainy

Authors 8/31/2015 3:38 PM
Deleted: of

Authors 8/31/2015 3:38 PM
Deleted: rainy

Authors 8/31/2015 3:38 PM
Deleted: rainy

Authors 8/31/2015 3:38 PM
Deleted: By comparing the distribution

Wang Zhan 9/7/2015 10:49 PM
Deleted: Figure 13

639 with respect to ΔSM . When a new rainy day is added ($3B42RT = 0$ mm/day, $3B42RT_{ADJ}$
640 > 0 mm/day) based on AMSR-E/LSMEM ΔSM of ≥ 2 mm/day, there's approximately 78%
641 chance that the added rain day is a true event (NLDAS > 0 mm/day); That is, approx.
642 22% chance that it is a false alarm (NLDAS = 0 mm/day). When AMSR-E/LSMEM
643 ΔSM is larger than 2 mm/day, the probability of added rainy days being true event is
644 even higher, up to 90% chance. Here we applied a threshold of 2 mm/day on AMSR-
645 E/LSMEM ΔSM . That is, when new rainy days are introduced ($3B42RT > 0$,
646 $3B42RT_{ADJ} \geq 0$), we discard the update and keep the no-rain day if AMSR-E/LSMEM
647 soil moisture increment is below 2 mm. Note that, the probability of the false alarms
648 depends on soil moisture climatology: the wetter soil moisture climatology, the larger
649 uncertainty in the signal. Therefore, this threshold should vary in accordance with local
650 soil moisture climatology, i.e. a larger threshold over the wetter east U.S. and smaller
651 threshold over the drier western U.S. Nevertheless, after the 2 mm/day ΔSM threshold is
652 applied, expectedly, the statistics are largely improved: FAR is decreased significantly
653 from 0.519 (w.o. ΔSM threshold) to 0.066 (w. ΔSM threshold). MAE of light rainfall (< 2
654 mm/day) in $3B42RT_{ADJ}$ decreased from 0.99 mm/day to 0.64 mm/day, compared to 0.65
655 mm/day in $3B42RT$. For medium to large $3B42RT$ rainfall (≥ 2 mm/day), it effectively
656 increased POD (0.362 in $3B42RT$ vs 0.386 in $3B42RT_{ADJ}$ w. ΔSM threshold) and
657 decreased FAR (0.037 in $3B42RT$ vs 0.030 in $3B42RT_{ADJ}$ w. ΔSM threshold). Further
658 work is needed to characterize, distinguish and decrease the high-frequency noise in SM
659 retrievals. Figure 13 gives an example of evaluating the impact of SM uncertainties in
660 assimilation as curves derived over different topography can be quantitatively compared.

661 5 Comparison to other studies

662 Many other studies have utilized satellite microwave brightness temperatures or soil
663 moisture retrievals to constrain satellite precipitation estimates (Pellarin et al., 2008),
664 estimate precipitation (e.g. Brocca et al., 2013) or improve precipitation estimates
665 through assimilation (Crow et al., 2009, 2011). Here, we review their approaches and
666 findings in light of the results of this study, and compare our results with some of these
667 studies to gain insight into their robustness and consistency.

Authors 8/31/2015 3:38 PM

Deleted: ΔSM

Authors 8/31/2015 3:38 PM

Deleted: falsely reported in $3B42RT_{ADJ}$, a cutoff ΔSM threshold of 2mm/day could filter out 99.8% of the false alarms. The simple application of a spatially uniform, stationary cutoff ΔSM threshold on the added rainy days could distinguish 3.3% of the true rain signals. The same evaluation metrics for

Authors 8/31/2015 3:38 PM

Deleted: after cutoff threshold is applied are provided in Figure 12c-d. Expectedly, the statistics are largely improved.

Authors 8/31/2015 3:38 PM

Formatted: Not Superscript/ Subscript

Authors 8/31/2015 3:38 PM

Deleted: rain amount

Authors 8/31/2015 3:38 PM

Deleted: Intensity-duration-frequency curves are also shown in Figure.A 2. Again, the difference in the performance of adjusted rainfall of selected grids is associated with local climatology. Thus

Authors 8/31/2015 3:38 PM

Deleted: However, it should also be noted that the application of the cutoff

Authors 8/31/2015 3:38 PM

Deleted: is not able to decrease uncertainties for

Authors 8/31/2015 3:38 PM

Deleted: .

Wang Zhan 9/7/2015 10:49 PM

Deleted: Figure 13

Authors 8/31/2015 3:38 PM

Deleted: analyzed the assimilation of

Authors 8/31/2015 3:38 PM

Deleted: to

Authors 8/31/2015 3:38 PM

Deleted: . In the following

Authors 8/31/2015 3:38 PM

Deleted: qualitatively

Authors 8/31/2015 3:38 PM

Moved up [1]: the effect of surface saturation on adjusted precipitation, which is well described in previous studies (e.g. Brocca et al.,

Authors 8/31/2015 3:38 PM

Deleted: Our results confirm

Authors 8/31/2015 3:38 PM

Deleted: 2011, 2013).

Deleted: In particular, Wanders et al. (2015, hereby W15) performed a comprehensive study using multiple satellite soil moisture (AMSR-E/LSMEM, ASCAT and SMOS) and land surface temperature data. This study focused exclusively on the usefulness of soil moisture product and differs in the pre-processing method (CDF-matching versus polynomial regression), the temporal period (2010-2011 versus 2002-2007) and the temporal resolution (3-hourly versus da... [5]

701 Pellarin et al. (2008) used the temporal variations of the AMSR-E 6.7 GHz brightness
702 temperature (TB) normalized polarization difference, $PR=(TB_V-TB_H)/(TB_V+TB_H)$, to
703 screen out anomalous precipitation events from a 4-day cumulative satellite-estimated
704 precipitation (EPSAT-SG: Chopin et al., 2005) from 22 to 26 of June 2004 over a 100 x
705 125 km box centered over Niger in west Africa. This was extended in Pellarin et al.
706 (2013) where an API-based water balance model was used to correct three different
707 satellite precipitation products (CMORPH, TRMM-3B42 and PERSIANN) over a 4-year
708 period in west Africa at three 0.25° grids in Niger, Benin and Mali). The new algorithm
709 was evaluated by comparing the corrected precipitation to estimates over the 0.25° grids
710 from ground-based precipitation measurements. A sequential assimilation approach was
711 applied where AMSR-E C-band TB measurements were used to estimate a simple
712 multiplicative factor to the precipitation estimates in order to minimize the difference
713 between observed (AMSR-E) and simulated TBs in term of root mean square error
714 (RMSE). The results show improvements over those found in Pellarin et al. (2009).
715 Specifically, the Pellarin et al. (2013) study shows that the proposed methodology
716 produces an improvement of the RMSE at daily, decadal and monthly time scales and at
717 the three locations. For instance, the RMS mean error decreases from 7.7 to 3.5 mm/day
718 at the daily time scale in Niger and from 18.3 to 7.7 mm/day at the decadal time scale in
719 Mali.

720 Crow et al. (2003, 2009, 2011) demonstrated the effectiveness of the assimilation of
721 remotely sensed microwave brightness temperatures or retrieved soil moisture in
722 estimating precipitation based on airborne measurements over the Southern Great Plains
723 (USA) region (Crow et al., 2003); 2 to 10 day accumulated precipitation within a simple
724 API water budget model and assimilation scheme over CONUS (Crow et al., 2009); and
725 3 day, 1° precipitation accumulation over three African Monsoon Multidisciplinary
726 Analysis (AMMA) sites in west Africa with an enhanced assimilation scheme and an
727 API-moisture model (Crow et al., 2011). Crow et al. (2009) recommends against
728 estimating precipitation at a larger scale than three days based on assimilating AMSR-
729 E/LSMEM soil moisture.

730 Brocca et al. (2013) estimated precipitation by inverting the water budget equation such
731 that precipitation could be estimated from changes in soil moisture. The inverted equation

744 [was calibrated using in-situ, 4-day averaged observations at two sites in Spain and Italy.](#)
745 [In Brocca et al. \(2014\), the same approach was used globally for 5-day precipitation](#)
746 [totals and at 1° spatially. Soil moisture observations from three satellite derived soil](#)
747 [moisture datasets \(AMSR-E LPRM, ASCAT and SMOS\) were used. The soil moisture](#)
748 [and rainfall were aggregated to a 1° spatial resolution, the soil moisture changes over a 5-](#)
749 [day period to estimate a 5-day total precipitation. No formal data assimilation was carried](#)
750 [out. The newly created precipitation data set was compared to two satellite precipitation](#)
751 [products \(TRMM-3B42RT, GPCC\) and two gauge based precipitation products \(GPCP,](#)
752 [ERA-Interim\). But they do note that their approach has “poor scores in reproducing daily](#)
753 [rainfall data”. Nonetheless, these studies show promising results.](#)

754 [In the study reported here, three advances have been made over these earlier studies: \(i\)](#)
755 [we adopted a state-of-the-art dynamic land surface model that has demonstrated high skill](#)
756 [in simulating soil moisture when driven by high quality precipitation data \(Schaake et al.,](#)
757 [2004\); \(ii\) we applied a state-of-the-art data assimilation procedure based on particle](#)
758 [filtering so as to extract \(and hopefully maximize\) the information content from the](#)
759 [satellite most effectively; \(iii\) we increased the resolution of the precipitation estimation](#)
760 [window down to 1 day, exceeding the conclusions in these earlier studies that the finest](#)
761 [temporal resolution is 3 to 5 days. Additionally we increased \(or matched\) the spatial](#)
762 [resolution to 0.25°, limited primarily by the satellite soil moisture product resolution; and](#)
763 [\(iv\) previous studies are based on the assumption that the SM retrievals are 100%](#)
764 [accurate and contain no errors. We evaluated this assumption by analyzing the impact of](#)
765 [uncertainties associated with the soil moisture retrievals. These advances offer important](#)
766 [benefits when satellite precipitation products are used for applications such as flood](#)
767 [forecasting. Admittedly by aggregating in space and time, the improvement is more](#)
768 [robust since some errors are averaged out. However improving satellite precipitation by](#)
769 [AMSR-E/LSMEM SM is not entirely without skill. In fact, it could effectively correct](#)
770 [rainfall with proper cautions given to local climatology where the assimilation is carried](#)
771 [out.](#)

772 [Wanders et al. \(2015\) performed a comprehensive inter-comparison study using multiple](#)
773 [satellite soil moisture and land surface temperature \(LST\) data at fine temporal scale \(3-](#)
774 [hourly\). Compared to their study, ours focuses on using soil moisture exclusively from](#)

775 one satellite and retrieval algorithm, and in improvements to the assimilation algorithm.
776 Specifically in (i) the longer temporal period (2010-2011 in Wanders, et al. versus 2002-
777 2007 in this study), (ii) the temporal resolution (3-hourly versus daily); (iii) the particle
778 generation and bias correction method. We present in the paper improvements in the
779 generation of rain particles and the bias-correction of the satellite soil moisture
780 observations, as well as enhancements to the assimilation algorithm to maximize the
781 information that can be gained from using soil moisture alone in adjusting precipitation.
782 Due to the very strong and complicated spatial structure of precipitation, that is non-
783 Gaussian and non-stationary in both time and space, a more advanced method is applied
784 to generate possible precipitation fields than used or presented in earlier studies or in
785 Wanders et al, (2015). Furthermore, a more advanced bias correction method is also
786 applied to account for the reported problems (Wanders et al., 2015) in the second order
787 statistics of the soil moisture retrievals; and (iv) SM retrieval products (and overpasses)
788 used in assimilation. Our improved results are based on soil moisture retrievals from
789 ascending overpasses only (versus both descending and ascending overpasses from
790 multiple datasets, i.e. AMSR-E/LSMEM, ASCAT and SMOS). Our exclusive focus on
791 the usefulness of soil moisture product promises more applicability especially for
792 improving satellite precipitation from the Global Precipitation Mission products. The
793 descending overpasses have generally better performance than the ascending, suggesting
794 the potentials of further improvements.

795 A quantitative comparison of Wanders et al. (2015) and our results is provided below.
796 Despite of the different time periods between Wanders et al. (2015, 2010-2011) and in
797 our study (2002-2007), Wanders et al. (2015) shows decreasing POD (-15.0% to -46.4%
798 depending on different products used) and FAR (-47.2% to -89.1% depending on
799 different products used) for all rainfall after assimilation, using either (single or multiple)
800 SM products alone or SM + LST data combined (see Table 4 of Wanders et al., 2015).
801 While in our study, after applying Δ SM threshold, medium to large 3B42RT_{ADJ} rainfall
802 (≥ 2 mm/day) has an increase in POD (+6.6%) and decrease in FAR (-18.9%).
803 Furthermore, the significant dry bias in adjusted precipitation (see Fig.6 of Wanders et
804 al., 2015) is not present in our results (Figure 9). This is due to improvements in our
805 precipitation ensemble generation and bias correction scheme. Wanders et al. (2015)

Authors 8/31/2015 3:38 PM

Deleted: ; however, W15

Authors 8/31/2015 3:38 PM

Deleted: and FAR

Authors 8/31/2015 3:38 PM

Deleted: .

Authors 8/31/2015 3:38 PM

Deleted: . W15

810 applied an additional step generating precipitation particles sampling from a 3×3 window,
811 that over-eliminates most of the excessive rainfall, along with some real signal. We
812 suggest loosening this constraint to a larger window size or to sample from adjusted
813 precipitation instead of original 3B42RT precipitation. However sampling from adjusted
814 precipitation at each time step, would significantly increase the computational demand,
815 limiting the potential for a global application at high temporal/spatial resolution.

816 Furthermore, the outcome is quite different for the distribution of soil moisture retrievals
817 after pre-processing (Fig.9 of Wanders et al. 2015 vs Figure 4 in our study) due to
818 different methods used. After pre-processing, distributions of soil moisture retrievals is
819 more similar to that of NLDAS precipitation forced, VIC modeled 1st layer soil moisture.
820 CDF-matching used by Wanders et al., (2015) is based on the assumption that satellite
821 soil moisture and modeled soil moisture respond to heavy rainfall in the same way,
822 essentially having a rank correlation of 1. However that is not observed because of
823 shallower detection depth of the satellite soil moisture. On the other hand, using the pre-
824 processing method presented in this study, the signal of near-saturation in AMSR-
825 E/LSMEM ΔSM tends to be overestimated after pre-processing, which indicates a heavy
826 rain event that is often accompanied with surface saturation, and thus does not provide
827 effective information for the assimilation. The other benefit of the 2nd order polynomial
828 regression lies in its non-linearity. An error in the soil moisture product impacts the
829 precipitation adjustment in a predictable way, allowing for a more systematic post-
830 processing treatment. Based on the known error characteristics, we demonstrate a
831 potential remedy to deal with the error by applying a 2 mm/day cutoff ΔSM threshold.
832 Meanwhile, it is also highlighted that the cutoff threshold should be variable and
833 positively correlated with local soil moisture climatology. We acknowledge that the soil
834 moisture product used in Wanders et al. (2015), is a blended product of multiple satellite
835 soil moisture datasets. It is not clear how its error characteristics impact the adjusted
836 precipitation.

837 6 Conclusion and Discussion

838 Based on the retrieved soil moisture from AMSR-E using the LSMEM retrieval
839 algorithm, we propose an assimilation procedure to integrate soil moisture information

Authors 8/31/2015 3:38 PM

Deleted: , which effectively filtered out

Authors 8/31/2015 3:38 PM

Deleted: . Note that applying such

Authors 8/31/2015 3:38 PM

Deleted: method, the independence of grid cells in VIC model is no longer maintained. This means that all grids need to be channeled after

Authors 8/31/2015 3:38 PM

Deleted: . Channeling grid cells

Authors 8/31/2015 3:38 PM

Deleted: computation efficiency

Authors 8/31/2015 3:38 PM

Formatted: Normal, No bullets or numbering

Authors 8/31/2015 3:38 PM

Deleted: when applying 0.1mm/day and 2mm/day event threshold (no significant increase in FAR for 2mm/day threshold); While in W15, decrease in both POD and FAR for 0mm/3hr and 2mm/3hr rain event threshold is reported. This is most likely due to the pre-processing method. CDF-matching

Wang Zhan 9/7/2015 10:49 PM

Deleted: Figure 4

Authors 8/31/2015 3:38 PM

Deleted: .

Authors 8/31/2015 3:38 PM

Deleted: true

Authors 8/31/2015 3:38 PM

Deleted: .

Authors 8/31/2015 3:38 PM

Deleted: in

Authors 8/31/2015 3:38 PM

Deleted: Error

Authors 8/31/2015 3:38 PM

Deleted: proper

Authors 8/31/2015 3:38 PM

Deleted: demonstrated

Authors 8/31/2015 3:38 PM

Deleted: 2mm

Authors 8/31/2015 3:38 PM

Deleted: W15

Authors 8/31/2015 3:38 PM

Deleted: model

866 into the VIC land surface model so as to improve real-time, satellite precipitation
867 estimates. The ability to estimate rainfall amount is now enhanced with the above
868 improvements, especially for [correcting](#) medium rainfall amounts. However, constrained
869 by the noise in [AMSR-E TBs and thus](#) soil moisture retrievals, the assimilation is not
870 effective in detecting missed rainfall events. The improved precipitation estimates,
871 referred to as 3B42RT_{ADJ} estimates, are overall consistent in reproducing the spatial
872 pattern and time series of daily rainfall from NLDAS precipitation. The results illustrate
873 the potential benefits of using data assimilation to merge satellite retrievals of surface soil
874 moisture into a land surface model forced with real-time precipitation. Potentially the
875 method can be applied globally for areas meeting vegetation cover and surface condition
876 constraints that allows for soil moisture retrievals. Under these conditions, the approach
877 can provide a supplementary source of information for enhancing the quality of satellite
878 rainfall estimation, especially over poorly gauged areas like Africa.

Authors 8/31/2015 3:38 PM

Deleted: correction

879 Nonetheless, some caution is required. The results of this study [show](#) that the adjusted
880 real-time precipitation tends to add additional rain (frequency) resulting in more time
881 steps with rain but lower regional average in the [western U.S.](#) and slightly higher regional
882 average in [the](#) eastern U.S. It is also noticed that the precipitation adjustments are
883 insensitive [under](#) saturated soil moisture conditions. A wetter surface magnifies any error
884 associated with satellite observation by incorrectly adjusting precipitation. These errors,
885 mixed with the “real” signal, generally add approximately ~2mm of precipitation (or
886 higher) depending on the soil moisture climatology. It is important to consider these
887 circumstances when observations are used so as to avoid introducing additional error.
888 With these identified limitations, continued research is needed to assess the biases in the
889 real-time precipitation retrievals on a local to regional basis so the assimilation system
890 can be modified accordingly.

Authors 8/31/2015 3:38 PM

Deleted: shows

Authors 8/31/2015 3:38 PM

Deleted: West

Authors 8/31/2015 3:38 PM

Deleted: with

891 The assimilation scheme used here assumed that the errors were attributed to the real-
892 time precipitation retrievals, but the precipitation estimates after adjustment includes
893 errors from additional sources. The two primary sources are errors in soil moisture
894 retrievals and errors in the land surface model that include model parameterizations
895 (poorly or insufficiently represented processes as well as scale issues) and parameter
896 errors (insufficient calibration). There are also errors in other model forcing fields besides

901 precipitation. Further studies are needed to assess the attribution of these error sources to
902 the total error. Such research will further improve the use of real-time satellite-based
903 precipitation for global flood monitoring.

904 Besides the clear, heavy dependency of the assimilation effectiveness on the accuracy of
905 satellite soil moisture product, it is also important to acquire adequate knowledge on the
906 error characteristics of satellite soil moisture retrievals. Knowledge of the soil moisture
907 errors could be important and the assimilation methods (including precipitation ensemble
908 generation and pre-/post-processing method) should be chosen accordingly. On the other
909 hand, the presence of data gaps between overpasses could be a large source of uncertainty
910 with data assimilation. Further effort towards reliable spatial-temporal continuous (gap
911 filled) satellite soil moisture datasets is needed.

912 While it has been illustrated in this study that the enhancement of real time satellite
913 precipitation estimates can be realized through an assimilation approach using satellite
914 soil moisture data products and a particle filter, additional satellite-based observations
915 (e.g. multi-sensor soil moisture products) or variables (e.g. land surface temperatures as
916 shown in Wanders et al. 2015, inundated areas), could be added/replaced in the
917 assimilation process with different levels of complexity; e.g. by applying constraints on
918 the particle generation. This opens up a great number of opportunities in using space-
919 borne observations for supplementing direct retrievals of precipitation.

920 Acknowledgements

921 This research was supported through NASA grant NNX13AG97G (Multi-sensor
922 enhancement of real-time satellite precipitation retrievals for improved drought
923 monitoring) under the Precipitation Measurement Mission. Part of this research was
924 financially supported by NWO Rubicon 825.15.003. This support is gratefully
925 acknowledged.

926

Authors 8/31/2015 3:38 PM

Deleted: on

Authors 8/31/2015 3:38 PM

Deleted: error

Authors 8/31/2015 3:38 PM

Deleted: in

Authors 8/31/2015 3:38 PM

Deleted: area

Authors 8/31/2015 3:38 PM

Deleted: apply constrains

Authors 8/31/2015 3:38 PM

Formatted: English (UK)

Authors 8/31/2015 3:38 PM

Deleted: Page Break

934 **References**

935 Brocca, L., Melone, F., Moramarco, T. and Morbidelli, R.: Antecedent wetness
936 conditions based on ERS scatterometer data, *J. Hydrol.*, 364(1-2), 73–87,
937 doi:10.1016/j.jhydrol.2008.10.007, 2009.

938 Brocca, L., Moramarco, T., Melone, F. and Wagner, W.: A new method for rainfall
939 estimation through soil moisture observations, *Geophys. Res. Lett.*, 40(5), 853–858,
940 doi:10.1002/grl.50173, 2013.

941 Brocca, L., Ciabatta, L., Massari, C., Moramarco, T., Hahn, S., Hasenauer, S., Kidd, R.,
942 Dorigo, W., Wagner, W. and Levizzani, V.: Soil as a natural rain gauge: Estimating
943 global rainfall from satellite soil moisture data, *J. Geophys. Res. Atmos.*, 119(9), 5128–
944 5141, doi:10.1002/2014JD021489, 2014.

945 [Chopin, F., Berges, J., Desbois, M., Jobard, I. and Lebel, T.: Satellite Rainfall Probability
946 and Estimation. Application to the West Africa During the 2004 Rainy Season, AGU
947 Spring Meet. Abstr., A12, 2005.](#)

948 Crow, W. T.: Correcting land surface model predictions for the impact of temporally
949 sparse rainfall rate measurements using an ensemble Kalman filter and surface brightness
950 temperature observations, *J. Hydrometeorol.*, 4(5), 960–973, 2003.

951 Crow, W. T., Huffman, G. J., Bindlish, R. and Jackson, T. J.: Improving Satellite-Based
952 Rainfall Accumulation Estimates Using Spaceborne Surface Soil Moisture Retrievals, *J.*
953 *Hydrometeorol.*, 10(1), 199–212, doi:10.1175/2008JHM986.1, 2009.

954 Crow, W. T., Van Den Berg, M. J., Huffman, G. J. and Pellarin, T.: Correcting rainfall
955 using satellite-based surface soil moisture retrievals: The Soil Moisture Analysis Rainfall
956 Tool (SMART), *Water Resour. Res.*, 47(8), 1–15, doi:10.1029/2011WR010576, 2011.

957 [Dee, D. P., Uppala, S. M., Simmons, A. J., Berrisford, P., Poli, P., Kobayashi, S., Andrae,
958 U., Balmaseda, M. A., Balsamo, G., Bauer, P. and others: The ERA-Interim reanalysis:
959 Configuration and performance of the data assimilation system, *Q. J. R. Meteorol. Soc.*,
960 \[137\\(656\\), 553–597, 2011.\]\(#\)](#)

961 Ebert, E. E., Janowiak, J. E. and Kidd, C.: Comparison of near-real-time precipitation
962 estimates from satellite observations and numerical models, *Bull. Am. Meteorol. Soc.*,
963 88(1), 47–64, doi:10.1175/BAMS-88-1-47, 2007.

964 Ek, M. B., Xia, Y., Wood, E., Sheffield, J., Luo, L., Lettenmaier, D., Livneh, B., Mocko,
965 D., Cosgrove, B., Meng, J., Wei, H., Koren, V., Schaake, J., Mo, K., Fan, Y. and Duan,
966 Q.: North American Land Data Assimilation System Phase 2 (NLDAS-2): Development
967 and Applications, *GEWEX Newsl.*, 21(2), 5–7, 2011.

968 Francois, C., Quesney, A. and Ottlé, C.: SAR Data into a Coupled Land Surface–
969 Hydrological Model Using an Extended Kalman Filter, *J. Hydrometeorol.*, 4(2), 473–487,
970 doi:10.1175/1525-7541(2003)4<473:SAOESD>2.0.CO;2, 2003.

971 Gao, H., Tang, Q., Shi, X., Zhu, C., Bohn, T. J., Su, F., She eld, J., Pan, M., and Wood,
972 E. F.: Water budget record from Variable Infiltration Capacity (VIC) model, in:
973 Algorithm Theoretical Basis Document for Terrestrial Water Cycle Data Records (in
974 review), 2010.

975 Huffman, G. J., Bolvin, D. T., Nelkin, E. J., Wolff, D. B., Adler, R. F., Gu, G., Hong, Y.,
976 Bowman, K. P. and Stocker, E. F.: The TRMM Multisatellite Precipitation Analysis
977 (TMPA): Quasi-Global, Multiyear, Combined-Sensor Precipitation Estimates at Fine
978 Scales, *J. Hydrometeorol.*, 8(1), 38–55, doi:10.1175/JHM560.1, 2007.

979 Huffman, G. J., Adler, R. F., Bolvin, D. T., and Nelkin, E. J.: The TRMM Multi-satellite
980 Precipitation Analysis (TMPA), in: *Satellite Rainfall Applications for Surface*
981 *Hydrology*, Springer Netherlands, 3–22, 2010.

982 Kalman, R. E.: A New Approach to Linear Filtering and Prediction Problems, *J. Basic*
983 *Eng.*, 82(1), 35, doi:10.1115/1.3662552, 1960.

984 [Kerr, Y. H., Waldteufel, P., Richaume, P., Wigneron, J.-P., Ferrazzoli, P., Mahmoodi, A.,](#)
985 [Al Bitar, A., Cabot, F., Gruhier, C., Juglea, S. E., Leroux, D., Mialon, A. and Delwart, S.:](#)
986 [The SMOS Soil Moisture Retrieval Algorithm, *Geosci. Remote Sensing, IEEE Trans.*,](#)
987 [50\(5\), 1384–1403, doi:10.1109/TGRS.2012.2184548, 2012.](#)

988 Liang, X., Lettenmaier, D. P., Wood, E. F. and Burges, S. J.: A simple hydrologically
989 based model of land surface water and energy fluxes for general circulation models, *J.*
990 *Geophys. Res.*, 99, 14415–14428, doi:10.1029/94JD00483, 1994.

991 Liang, X., Wood, E. F. and Lettenmaier, D. P.: Surface soil moisture parameterization of
992 the VIC-2L model: Evaluation and modification, *Glob. Planet. Change*, 13(1-4), 195–
993 206, doi:10.1016/0921-8181(95)00046-1, 1996.

994 Massari, C., Brocca, L., Moramarco, T., Tramblay, Y. and Didon Lescot, J.-F.: Potential
995 of soil moisture observations in flood modelling: estimating initial conditions and
996 correcting rainfall, *Adv. Water Resour.*, 74, 44–53, doi:10.1016/j.advwatres.2014.08.004,
997 2014.

998 Matgen, P., Fenicia, F., Heitz, S., Plaza, D., de Keyser, R., Pauwels, V. R. N., Wagner,
999 W. and Savenije, H.: Can ASCAT-derived soil wetness indices reduce predictive
1000 uncertainty in well-gauged areas? A comparison with in situ observed soil moisture in an
1001 assimilation application, *Adv. Water Resour.*, 44, 49–65,
1002 doi:10.1016/j.advwatres.2012.03.022, 2012.

1003 McCabe, M. F., Wood, E. F. and Gao, H.: Initial soil moisture retrievals from AMSR-E:
1004 Multiscale comparison using in situ data and rainfall patterns over Iowa, *Geophys. Res.*
1005 *Let.*, 32(6), 1–4, doi:10.1029/2004GL021222, 2005.

1006 Pan, M. and Wood, E. F.: Data Assimilation for Estimating the Terrestrial Water Budget
1007 Using a Constrained Ensemble Kalman Filter, *J. Hydrometeorol.*, 7(3), 534–547,
1008 doi:10.1175/JHM495.1, 2006.

1009 Pan, M., Li, H. and Wood, E.: Assessing the skill of satellite-based precipitation
1010 estimates in hydrologic applications, *Water Resour. Res.*, 46(9), W09535,
1011 doi:10.1029/2009WR008290, 2010.

1012 Pan, M., Sahoo, A. K. and Wood, E. F.: Improving soil moisture retrievals from a
1013 physically-based radiative transfer model, *Remote Sens. Environ.*, 140, 130–140,
1014 doi:10.1016/j.rse.2013.08.020, 2014.

1015 Pellarin, T., Ali, A., Chopin, F., Jobard, I. and Bergès, J. C.: Using spaceborne surface
 1016 soil moisture to constrain satellite precipitation estimates over West Africa, *Geophys.*
 1017 *Res. Lett.*, 35(2), 3–7, doi:10.1029/2007GL032243, 2008.

1018 Pellarin, T., Louvet, S., Gruhier, C., Quantin, G. and Legout, C.: A simple and effective
 1019 method for correcting soil moisture and precipitation estimates using AMSR-E
 1020 measurements, *Remote Sens. Environ.*, 136, 28–36, doi:10.1016/j.rse.2013.04.011, 2013.

1021 Robock, A., Luo, L., Wood, E. F., Wen, F., Mitchell, K., Houser, P., Schaake, J.,
 1022 Lohmann, D., Cosgrove, B., Sheffield, J., Duan, Q., Higgins, W., Pinker, R., Tarpley, D.,
 1023 Basara, J. and Crawford, K.: Evaluation of the North American Land Data Assimilation
 1024 System over the southern Great Plains during the warm season, *J. Geophys. Res.*,
 1025 108(D22), 8846, doi:10.1029/2002JD003245, 2003.

1026 Schaake, J. C., Duan, Q., Koren, V., Mitchell, K. E., Houser, P. R., Wood, E. F., Robock,
 1027 A., Lettenmaier, D. P., Lohmann, D., Cosgrove, B., Sheffield, J., Luo, L., Higgins, R. W.,
 1028 Pinker, R. T., and Tarpley, J. D.: An intercomparison of soil moisture fields in the North
 1029 American Land Data Assimilation System (NLDAS), *J. Geophys. Res. Atmos.*, 109(D1),
 1030 doi:10.1029/2002JD003309, 2004.

1031 Schamm, K., M. Ziese, A. Becker, P. Finger, A. Meyer-Christoffer, U. Schneider, M.
 1032 Schröder, and P. Stender (2014), Global gridded precipitation over land: A description of
 1033 the new GPCP First Guess Daily product, *Earth Syst. Sci. Data*, 6, 49–60

1034 Sorooshian, S.: Commentary-GEWEX (Global Energy and Water Cycle Experiment) at
 1035 the 2004 Joint Scientific Committee Meeting, *GEWEX Newsl.*, 14(2), 2, 2004.

1036 Wanders, N., Pan, M. and Wood, E. F.: Correction of real-time satellite precipitation with
 1037 multi-sensor satellite observations of land surface variables, *Remote Sens. Environ.*, 160,
 1038 206–221, doi:10.1016/j.rse.2015.01.016, 2015.

1039 Wu, H., Adler, R. F., Tian, Y., Huffman, G. J., Li, H. and Wang, J.: Real-time global
 1040 flood estimation using satellite-based precipitation and a coupled land surface and routing
 1041 model. *Water Resour. Res.*, 50(3), 2693-2717, doi:10.1002/2013WR014710, 2014.

1042

Authors 8/31/2015 3:38 PM
 Deleted: . Y

Authors 8/31/2015 3:38 PM
 Moved (insertion) [2]

Authors 8/31/2015 3:38 PM
 Moved (insertion) [3]

Authors 8/31/2015 3:38 PM
 Moved (insertion) [4]

Authors 8/31/2015 3:38 PM
 Moved (insertion) [5]

Authors 8/31/2015 3:38 PM
 Moved up [2]: Robock, A., Lettenmaier, D. P., Lohmann, D., Cosgrove, B.,

Authors 8/31/2015 3:38 PM
 Moved up [3]: Higgins, R. W., Pinker, R. T

Authors 8/31/2015 3:38 PM
 Deleted: .,

Authors 8/31/2015 3:38 PM
 Moved up [4]: and Tarpley, J. D.: An intercomparison of soil moisture fields in the North American Land Data

Authors 8/31/2015 3:38 PM
 Moved up [5]: Geophys.

Authors 8/31/2015 3:38 PM
 Deleted: She eld, J., Luo, L. F.,

Authors 8/31/2015 3:38 PM
 Deleted: Assimilation System (NLDAS), J.

Authors 8/31/2015 3:38 PM
 Deleted: Res., 109(D1), D01S90, doi:10.1029/2002JD003309, 2004. .

Authors 8/31/2015 3:38 PM
 Deleted: ————— Page Break —————

1058 [List of Tables](#)

1059 [Tables](#)

1060 [Table 1 Error statistics of recovered precipitation and effect of surface saturation in the idealized experiment \(mm/day\)](#)

1061 [Table 2 Error statistics of recovered NLDAS based on \$\Delta\$ SM \(with added errors\) conditioned on 1st layer soil wetness for the idealized](#)
1062 [experiment \(mm/day\)](#)

1063 [Table 3 Error statistics of 3B42RT and 3B42RT_{ADJ} compared to NLDAS precipitation \(mm/day\)](#)

Authors 8/31/2015 3:38 PM

Deleted:

Unknown

Formatted: Font:(Default) Helvetica, 6 pt

Wang Zhan 9/7/2015 10:49 PM

Deleted: Tables -

... [6]

Wang Zhan 9/7/2015 10:49 PM

Deleted: Table 2 Error statistics of recovered NLDAS based on Δ SM (with added errors) conditioned on 1st layer soil wetness for the idealized experiment (mm/day).

Wang Zhan 9/7/2015 10:49 PM

Deleted: Table 3 Error statistics of 3B42RT and 3B42RT_{ADJ} compared to NLDAS precipitation (mm/day)

1074 **List of Figures**

1075 Figure 1 Schematic for the dynamic assimilation of AMSR-E/LSMEM Δ SM into TMPA

1076 (3B42RT) with the particle filter (PF).

1077 Figure 2 Schematic for the strategy for processing prior and posterior probability

1078 densities in the particle filter.

1079 Figure 3 Statistics of NLDAS precipitation given 3B42RT precipitation measurement.

1080 Boxplot shows the minimum, 15% quantile, 30% quantile, median, 70% quantile, 85%

1081 quantile and maximum value of NLDAS precipitation given 3B42RT precipitation in a

1082 certain bin.

1083 Figure 4 Empirical cumulative distribution function of changes in soil moisture from top

1084 layer soil moisture from NLDAS precipitation forced VIC simulation (black), and

1085 AMSR-E/LSMEM soil moisture retrieval before (red) and after (blue) pre-processing.

1086 Figure 5 Two cases with recovered spatial rainfall pattern in the idealized experiment

1087 after merging satellite soil moisture retrieval on: (a-e) 27th Oct. 2003 and (f-j) 22th Mar.

1088 2006.

1089 Figure 6 Accuracy of recovered precipitation in idealized experiment: (a) overall

1090 performance and separately comparing the improvement performance of recovered

1091 NLDAS precipitation (b) with and (c) without surface saturation condition. Statistics

1092 provided in Table 1.

1093 Figure 7 Error in recovered NLDAS precipitation given surface moisture condition.

1094 Recovered NLDAS is based on using “truth” soil moisture and soil moisture with normal

1095 error: N(0,1mm), N(0,2mm), N(0,3mm), N(0,4mm) and N(0,5mm). Statistics provided in

1096 Table 2.

Wang Zhan 9/7/2015 10:49 PM

Deleted: Figure 1 Schematic for the dynamic assimilation of AMSR-E/LSMEM Δ SM into TMPA (3B42RT) with the particle filter (PF).

Wang Zhan 9/7/2015 10:49 PM

Deleted: Figure 2 Schematic for the strategy for processing prior and posterior probability densities in the particle filter.

Wang Zhan 9/7/2015 10:49 PM

Deleted: Figure 3 Statistics of NLDAS precipitation given 3B42RT precipitation measurement. Boxplot shows the minimum, 15% quantile, 30% quantile, median, 70% quantile, 85% quantile and maximum value of NLDAS precipitation given 3B42RT precipitation in a certain bin.

Wang Zhan 9/7/2015 10:49 PM

Deleted: Figure 4 Empirical cumulative distribution function of changes in soil moisture from top layer soil moisture from NLDAS precipitation forced VIC simulation (black), and AMSR-E/LSMEM soil moisture retrieval before (red) and after (blue) pre-processing.

Wang Zhan 9/7/2015 10:49 PM

Deleted: Figure 5 Two cases with recovered spatial rainfall pattern in the idealized experiment after merging satellite soil moisture retrieval on: (a-e) 27th Oct. 2003 and (f-j) 22th Mar. 2006.

Wang Zhan 9/7/2015 10:49 PM

Deleted: Figure 6 Accuracy of recovered precipitation in idealized experiment: (a) overall performance and separately comparing the improvement performance of recovered NLDAS precipitation (b) with and (c) without surface saturation condition. Statistics provided in Table 1.

Wang Zhan 9/7/2015 10:49 PM

Deleted: Figure 7 Error in recovered NLDAS precipitation given surface moisture condition. Recovered NLDAS is based on using “truth” soil moisture and soil moisture with normal error: N(0,1mm), N(0,2mm), N(0,3mm), N(0,4mm) and N(0,5mm). Statistics provided in Table 2.

1136 [Figure 8 May 26th 2006 Rainfall pattern in 3B42RT \(b\) against NLDAS \(d\) as detected](#)
 1137 [by AMSR-E/LSMEM \$\Delta\$ SM \(a\), and recovered rainfall field \(3B42RT_{ADJ}\) by assimilating](#)
 1138 [AMSR-E/LSMEM \$\Delta\$ SM \(c\). Gray shading shows area without soil moisture retrievals.](#)
 1139 [Figure 9 Pearson correlation coefficient between AMSR-E/LSMEM \$\Delta\$ SM and](#)
 1140 [precipitation: a\) NLDAS, b\) 3B42RT and c\) 3B42RT_{ADJ}; annual mean precipitation in d\)](#)
 1141 [NLDAS, e\) 3B42RT and f\) 3B42RT_{ADJ} of time steps with AMSR-E/LSMEM \$\Delta\$ SM](#)
 1142 [retrievals.](#)
 1143 [Figure 10 Frequency of rainy days in 3B42RT, 3B42RT_{ADJ} and NLDAS with a\) 0.1](#)
 1144 [mm/day and b\) 2 mm/day rainfall threshold to define a rain day.](#)
 1145 [Figure 11 Distribution of 3B42RT and 3B42RT_{ADJ} precipitation error compared to](#)
 1146 [NLDAS. Statistics are provided in Table 3.](#)
 1147 [Figure 12 FAR and POD of 3B42RT and 3B42RT_{ADJ} with a\) 0.1 mm/day and b\) 2](#)
 1148 [mm/day rainfall threshold to define a rain event.](#)
 1149 [Figure 13 Probability that the added rainy days \(3B42RT = 0 mm/day, 3B42RT_{ADJ} > 0](#)
 1150 [mm/day\) are true rain events \(NLDAS > 0 mm/day\) given corresponding AMSR-](#)
 1151 [E/LSMEM \$\Delta\$ SM.](#)
 1152

Wang Zhan 9/7/2015 10:49 PM
Deleted: Figure 8 May 26th 2006 Rainfall pattern in 3B42RT (b) against NLDAS (d) as detected by AMSR-E/LSMEM Δ SM (a), and recovered rainfall field (3B42RT_{ADJ}) by assimilating AMSR-E/LSMEM Δ SM (c). Gray shading shows area without soil moisture retrievals.

Wang Zhan 9/7/2015 10:49 PM
Deleted: Figure 9 Pearson correlation coefficient between AMSR-E/LSMEM Δ SM and precipitation: a) NLDAS, b) 3B42RT and c) 3B42RT_{ADJ}; annual mean precipitation in d) NLDAS, e) 3B42RT and f) 3B42RT_{ADJ} of time steps with AMSR-E/LSMEM Δ SM retrievals.

Wang Zhan 9/7/2015 10:49 PM
Deleted: Figure 10 Frequency of rainy days in 3B42RT, 3B42RT_{ADJ} and NLDAS with a) 0.1 mm/day and b) 2 mm/day rainfall threshold to define a rain day.

Wang Zhan 9/7/2015 10:49 PM
Deleted: Figure 11 Distribution of 3B42RT and 3B42RT_{ADJ} precipitation error compared to NLDAS. Statistics are provided in Table 3.

Wang Zhan 9/7/2015 10:49 PM
Deleted: Figure 12 FAR and POD of 3B42RT and 3B42RT_{ADJ} with a) 0.1 mm/day and b) 2 mm/day rainfall threshold to define a rain event.

Wang Zhan 9/7/2015 10:49 PM
Deleted: Figure 13 Probability that the added rainy days (3B42RT = 0 mm/day, 3B42RT_{ADJ} > 0 mm/day) are true rain events (NLDAS > 0 mm/day) given corresponding AMSR-E/LSMEM Δ SM.

Tables

Table 1 Error statistics of recovered precipitation and effect of surface saturation in the idealized experiment (mm/day).

		0	0~0.2	0.2~0.5	0.5~1.0	1.0~1.5	1.5~2	2~2.5	2.5~5.0	5.0~7.5	7.5~10	10~15	15~20	20~25	>25
[Recovered NLDAS]-[NLDAS]															
All surface conditions	Bias	0.24	0.20	0.37	0.51	0.71	0.87	1.09	0.67	1.16	1.30	2.51	3.32	3.75	3.95
	MAE	0.40	0.42	0.66	0.86	1.14	1.41	1.70	1.48	2.24	2.63	4.21	5.56	6.70	9.76
Unsaturated surface	Bias	0.23	0.19	0.29	0.40	0.52	0.68	0.82	0.65	1.10	1.27	2.19	2.88	3.14	3.14
	MAE	0.39	0.41	0.59	0.75	0.95	1.21	1.43	1.45	2.17	2.58	3.88	5.11	6.07	8.94
Saturated surface	Bias	2.31	5.06	47.65	42.58	50.67	44.09	59.64	6.83	16.09	9.19	46.47	57.98	65.33	64.09
	MAE	3.35	5.54	48.71	43.73	52.43	46.96	61.85	9.64	21.42	15.01	49.07	60.78	69.53	70.73

Deleted: <sp>

Unknown

Formatted ... [7]

Authors 8/31/2015 3:38 PM

Formatted Table ... [8]

Authors 8/31/2015 3:38 PM

Formatted ... [9]

Authors 8/31/2015 3:38 PM

Formatted ... [10]

Authors 8/31/2015 3:38 PM

Formatted ... [11]

Authors 8/31/2015 3:38 PM

Formatted ... [19]

Authors 8/31/2015 3:38 PM

Formatted ... [12]

Authors 8/31/2015 3:38 PM

Formatted ... [13]

Authors 8/31/2015 3:38 PM

Formatted ... [14]

Authors 8/31/2015 3:38 PM

Formatted ... [15]

Authors 8/31/2015 3:38 PM

Formatted ... [16]

Authors 8/31/2015 3:38 PM

Formatted ... [17]

Authors 8/31/2015 3:38 PM

Formatted ... [18]

Authors 8/31/2015 3:38 PM

Formatted ... [20]

Authors 8/31/2015 3:38 PM

Formatted ... [21]

Authors 8/31/2015 3:38 PM

Formatted ... [22]

Authors 8/31/2015 3:38 PM

Formatted ... [23]

Authors 8/31/2015 3:38 PM

Deleted: 092

Authors 8/31/2015 3:38 PM

Deleted: 155

Authors 8/31/2015 3:38 PM

Formatted ... [24]

Authors 8/31/2015 3:38 PM

Deleted: 238

Authors 8/31/2015 3:38 PM

Formatted ... [25]

Authors 8/31/2015 3:38 PM

Formatted ... [26]

Authors 8/31/2015 3:38 PM

Authors 8/31/2015 3:38 PM

Formatted ... [27]

Authors 8/31/2015 3:38 PM

Formatted ... [28]

Table 2 Error statistics of recovered NLDAS based on ΔSM (with added errors) conditioned on 1st layer soil wetness for the idealized experiment (mm/day).

	[VIC 1st layer SM] - [maximum]*	<-30	-30~-25	-25~-20	-20~-15	-15~-12	-12~-10	-10~-9	-9~-8	>-8
[Recovered NLDAS]-[NLDAS] [mm/day]										
No error	Median	0.04	0.03	0.02	0.02	0.02	0.03	0.03	0.04	0.16
	IQR	0.14	0.08	0.07	0.07	0.08	0.12	0.21	0.29	1.71
1.0	Median	0.86	1.07	1.08	1.03	0.99	0.97	0.97	0.94	0.66
	IQR	1.52	1.72	1.77	1.83	1.96	2.08	2.14	2.19	2.59
2.0	Median	0.68	1.07	1.40	1.56	1.52	1.44	1.51	1.64	1.54
	IQR	1.76	2.09	2.88	3.45	3.63	3.73	3.73	3.73	3.91
3.0	Median	0.15	0.80	1.20	1.41	1.47	1.51	1.65	1.84	1.88
	IQR	1.36	2.16	3.04	3.73	3.74	3.79	4.34	5.24	5.47
4.0	Median	0.22	0.56	0.83	1.15	1.30	1.40	1.63	1.88	1.97
	IQR	0.99	2.36	2.48	3.99	4.05	4.70	5.53	5.52	5.63
5.0	Median	0.00	0.15	0.52	0.90	1.10	1.27	1.54	1.81	1.89
	IQR	1.62	2.54	2.91	4.43	4.51	5.95	5.90	5.79	7.04

*1st layer soil depth is 100mm with a SM capacity of ~45mm depending on porosity.

Formatted ... [117]

Authors 8/31/2015 3:38 PM

Deleted: <sp> - ... [118]

Unknown

Formatted ... [119]

Authors 8/31/2015 3:38 PM

Formatted Table ... [120]

Unknown

Formatted ... [121]

Authors 8/31/2015 3:38 PM

Formatted ... [122]

Authors 8/31/2015 3:38 PM

Formatted ... [123]

Authors 8/31/2015 3:38 PM

Formatted ... [124]

Authors 8/31/2015 3:38 PM

Formatted ... [125]

Authors 8/31/2015 3:38 PM

Formatted ... [126]

Authors 8/31/2015 3:38 PM

Formatted ... [127]

Authors 8/31/2015 3:38 PM

Formatted ... [128]

Authors 8/31/2015 3:38 PM

Formatted ... [129]

Authors 8/31/2015 3:38 PM

Formatted ... [130]

Deleted: 035

Authors 8/31/2015 3:38 PM

Deleted: 041

Authors 8/31/2015 3:38 PM

Formatted ... [141]

Authors 8/31/2015 3:38 PM

Deleted: 159

Authors 8/31/2015 3:38 PM

Formatted ... [134]

Authors 8/31/2015 3:38 PM

Deleted: 027

Authors 8/31/2015 3:38 PM

Deleted: 023

Authors 8/31/2015 3:38 PM

Formatted ... [135]

Authors 8/31/2015 3:38 PM

Deleted: 019

Authors 8/31/2015 3:38 PM

Formatted ... [137]

Authors 8/31/2015 3:38 PM

Formatted ... [131]

Authors 8/31/2015 3:38 PM

Formatted

Table 3 Error statistics of 3B42RT and 3B42RT_{ADJ} compared to NLDAS precipitation (mm/day)

[3B42RT] - [NLDAS] [mm/day]	<-25	-25~-	-20~-	-15~-	-10~-	-5~-2	-2~-	-	0.5~2	2~5	5~10	10~1	15~2	20~2	>25
	20	15	10	5	0.5	0.5~0	.5					5	0	5	
[3B42RT] - Mean	-32.32	-22.19	-17.13	-12.09	-6.98	-3.22	-1.09	-0.02	1.11	3.20	6.87	11.96	16.97	21.95	27.35
[NLDAS] STD	8.52	1.42	1.42	1.42	1.39	0.85	0.43	0.12	0.43	0.84	1.37	1.39	1.37	1.38	2.08
[3B42RT _{ADJ}] - Mean	-31.24	-20.31	-14.79	-9.69	-4.81	-1.60	0.16	1.08	0.44	0.21	0.02	-0.06	0.00	-0.03	-0.12
[NLDAS] STD	11.03	6.40	6.12	5.34	4.08	2.73	1.88	1.18	1.86	2.29	2.60	2.91	3.01	2.74	2.41

Formatted ... [249]

Authors 8/31/2015 3:38 PM

Formatted ... [269]

Authors 8/31/2015 3:38 PM

Formatted ... [250]

Authors 8/31/2015 3:38 PM

Formatted ... [253]

Authors 8/31/2015 3:38 PM

Formatted ... [254]

Authors 8/31/2015 3:38 PM

Formatted ... [255]

Authors 8/31/2015 3:38 PM

Formatted ... [266]

Authors 8/31/2015 3:38 PM

Formatted ... [267]

Authors 8/31/2015 3:38 PM

Formatted ... [256]

Authors 8/31/2015 3:38 PM

Formatted ... [257]

Authors 8/31/2015 3:38 PM

Formatted ... [259]

Authors 8/31/2015 3:38 PM

Formatted ... [260]

Authors 8/31/2015 3:38 PM

Formatted ... [262]

Authors 8/31/2015 3:38 PM

Formatted ... [264]

Authors 8/31/2015 3:38 PM

Formatted ... [265]

Authors 8/31/2015 3:38 PM

Formatted Table ... [251]

Authors 8/31/2015 3:38 PM

Formatted ... [263]

Authors 8/31/2015 3:38 PM

Formatted ... [268]

Authors 8/31/2015 3:38 PM

Formatted ... [270]

Authors 8/31/2015 3:38 PM

Formatted ... [271]

Authors 8/31/2015 3:38 PM

Formatted ... [272]

Authors 8/31/2015 3:38 PM

Formatted ... [274]

Authors 8/31/2015 3:38 PM

Formatted ... [275]

Authors 8/31/2015 3:38 PM

Formatted ... [277]

Authors 8/31/2015 3:38 PM

Formatted ... [252]

Authors 8/31/2015 3:38 PM

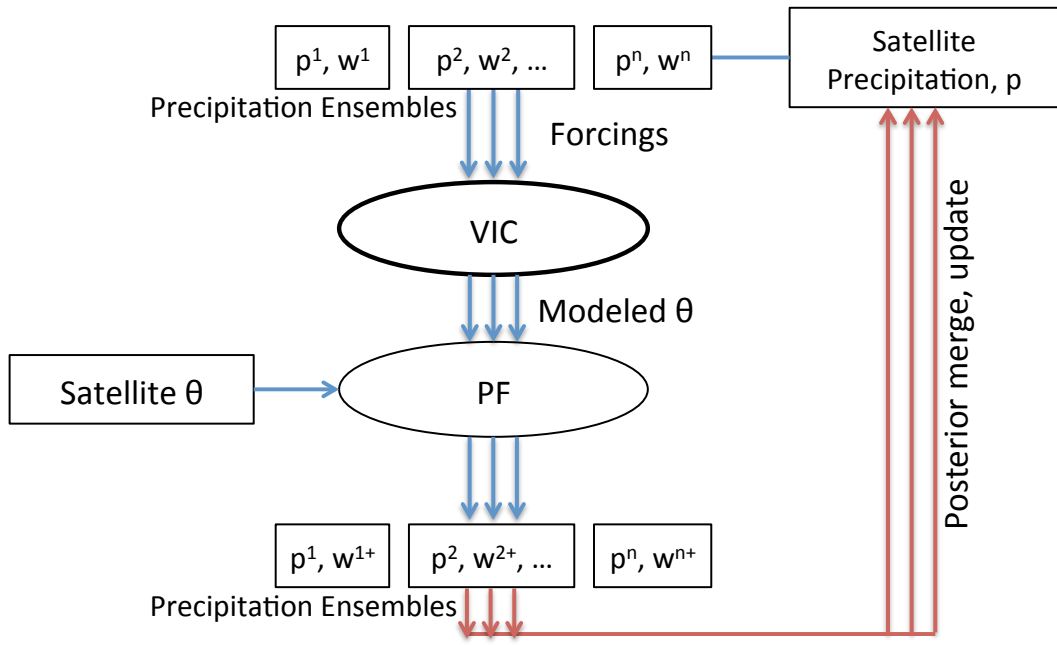
Formatted ... [258]

Authors 8/31/2015 3:38 PM

Formatted ... [261]

Authors 8/31/2015 3:38 PM

Formatted ... [273]



1710

1711 Figure 1 Schematic for the dynamic assimilation of AMSR-E/LSMEM Δ SM into TMPA (3B42RT) with the particle filter (PF).

1712

Authors 8/31/2015 3:38 PM

p^1, w^1
Precipitation Er

Satellite θ

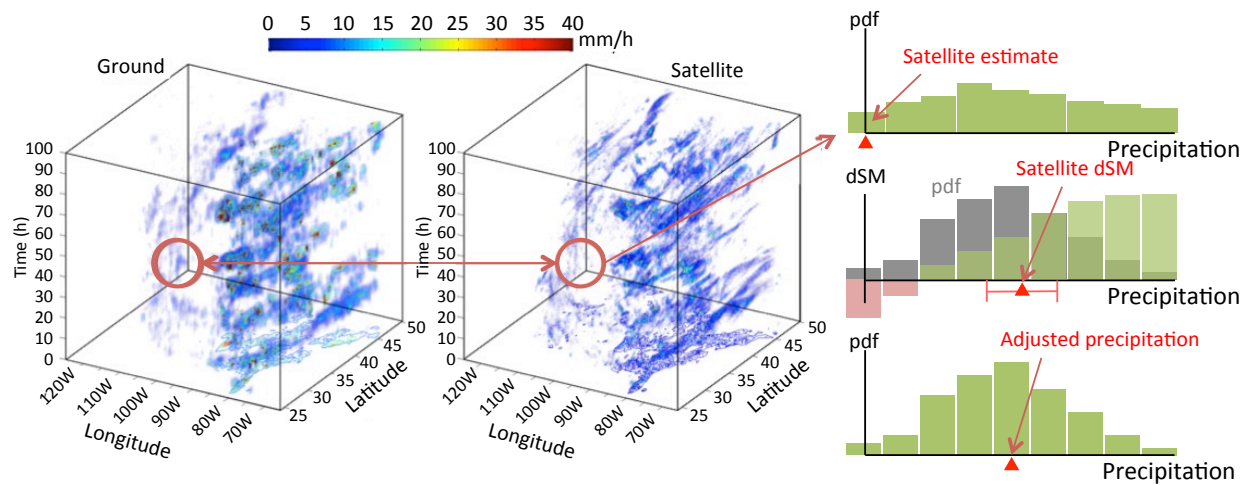
p^1, w^1
Precipitation Er

Deleted:

Authors 8/31/2015 3:38 PM
Deleted: of particle filtering

Authors 8/31/2015 3:38 PM
Deleted: Page Break

... [345]

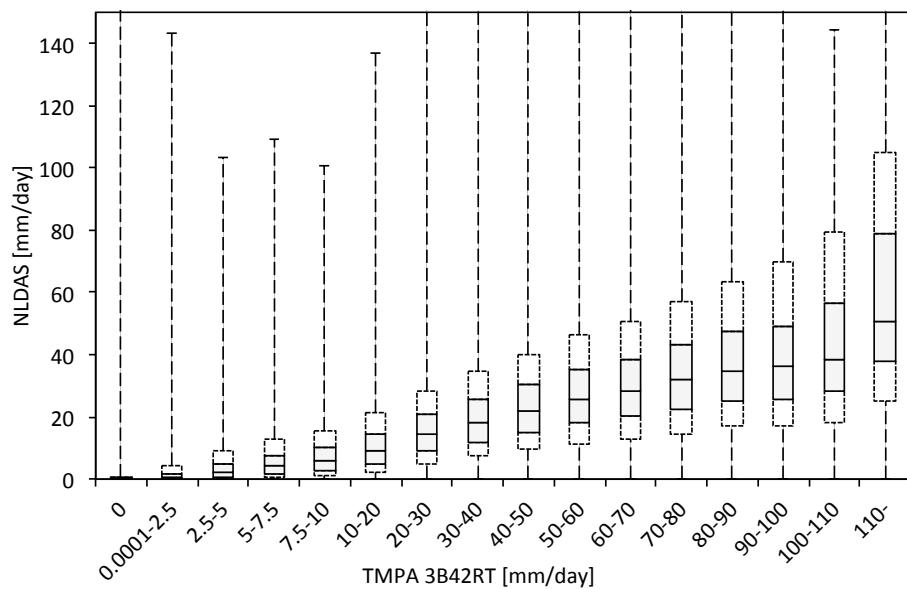


1718

1719 Figure 2 Schematic for [the strategy for processing](#) prior and posterior probability [densities](#) in [the](#) particle filter.

1720

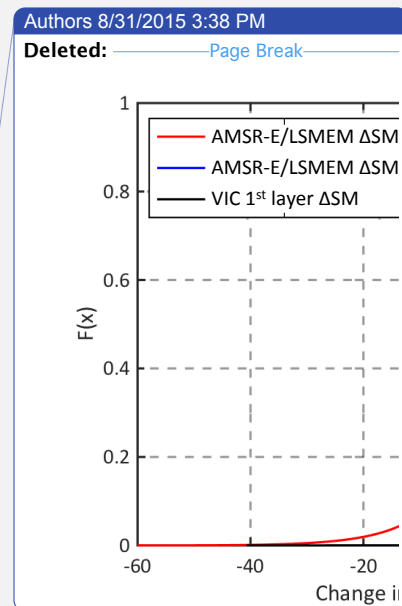
Authors 8/31/2015 3:38 PM
Deleted: handling
 Authors 8/31/2015 3:38 PM
Deleted: density handling strategy
 Authors 8/31/2015 3:38 PM
Deleted: Page Break
 ... [346]

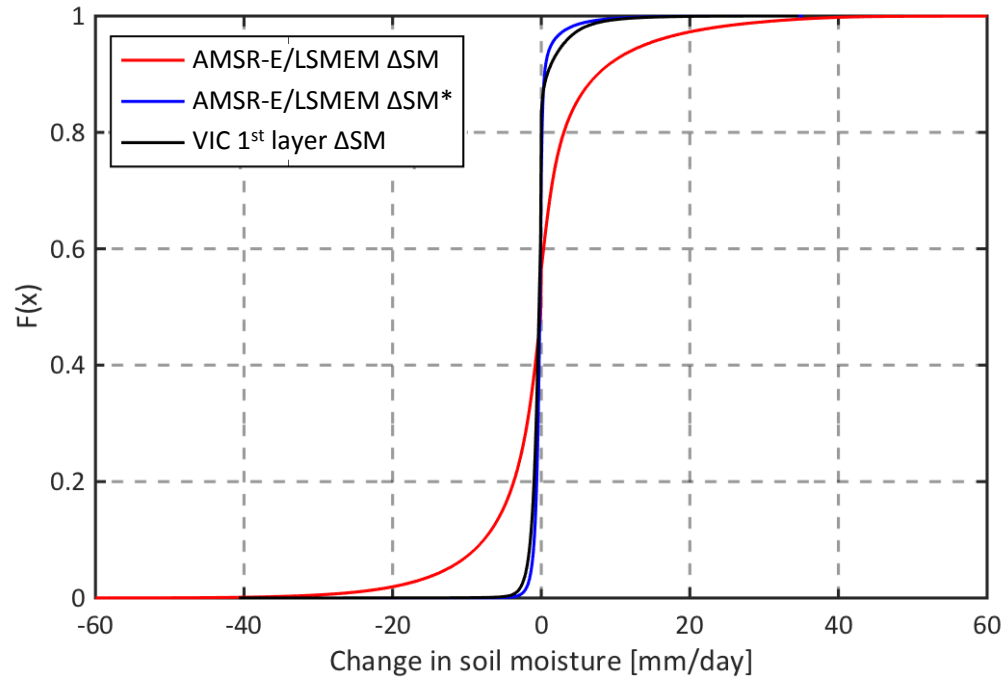


1726

1727 Figure 3 Statistics of NLDAS precipitation given 3B42RT precipitation measurement. Boxplot shows the minimum, 15% quantile,
 1728 30% quantile, median, 70% quantile, 85% quantile and maximum value of NLDAS precipitation given 3B42RT precipitation in a
 1729 certain bin.

1730



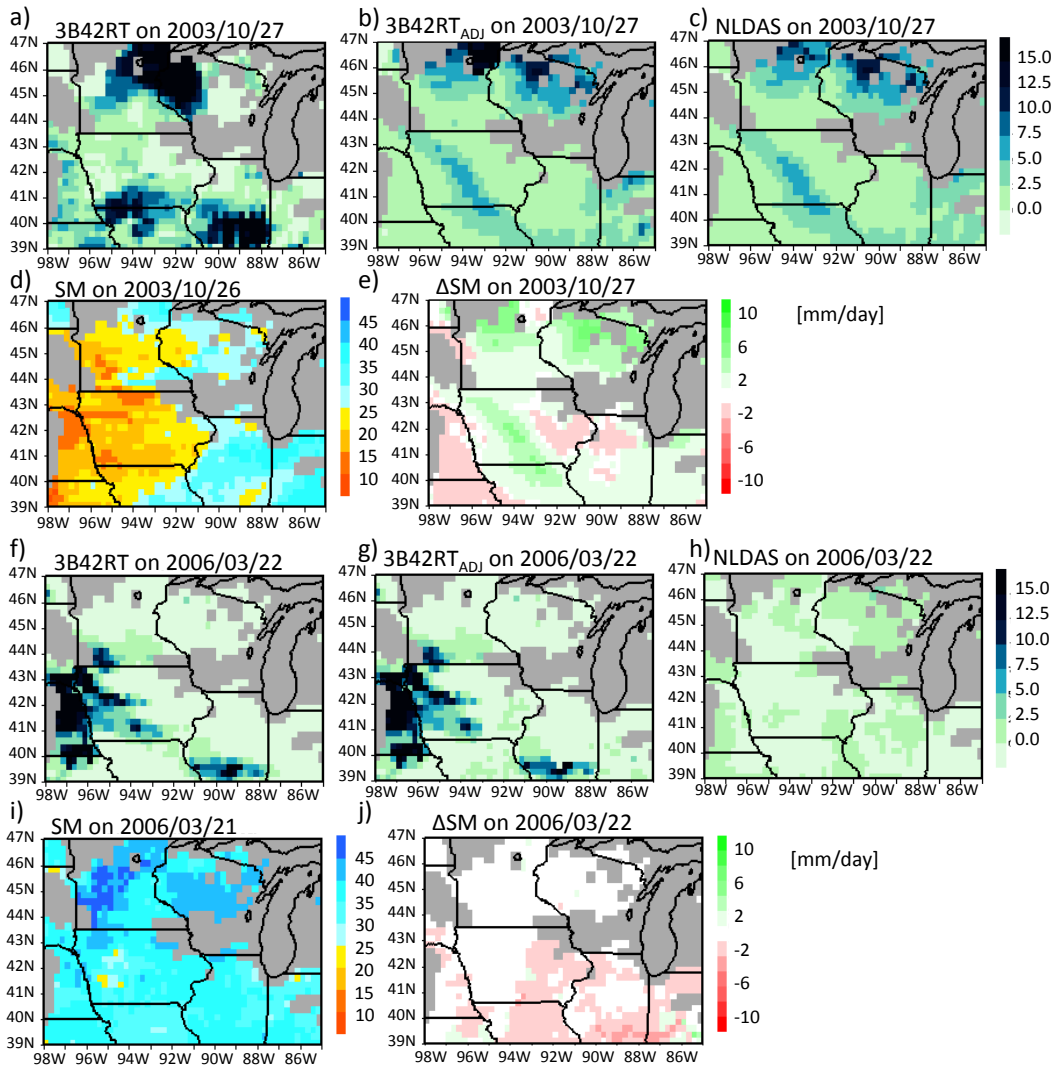


1733

1734 Figure 4 Empirical cumulative distribution function of changes in soil moisture from top layer soil moisture from NLDAS
 1735 precipitation forced VIC simulation (black), and AMSR-E/LSMEM soil moisture retrieval before (red) and after (blue) pre-
 1736 processing.

1737

Authors 8/31/2015 3:38 PM
 Deleted: Page Break
 ... [347]



741

742 Figure 5 Two cases with recovered spatial rainfall pattern in [the](#) idealized experiment after merging satellite
 743 soil moisture retrieval on: (a-e) 27th Oct. 2003 and (f-j) 22th Mar. 2006.

744

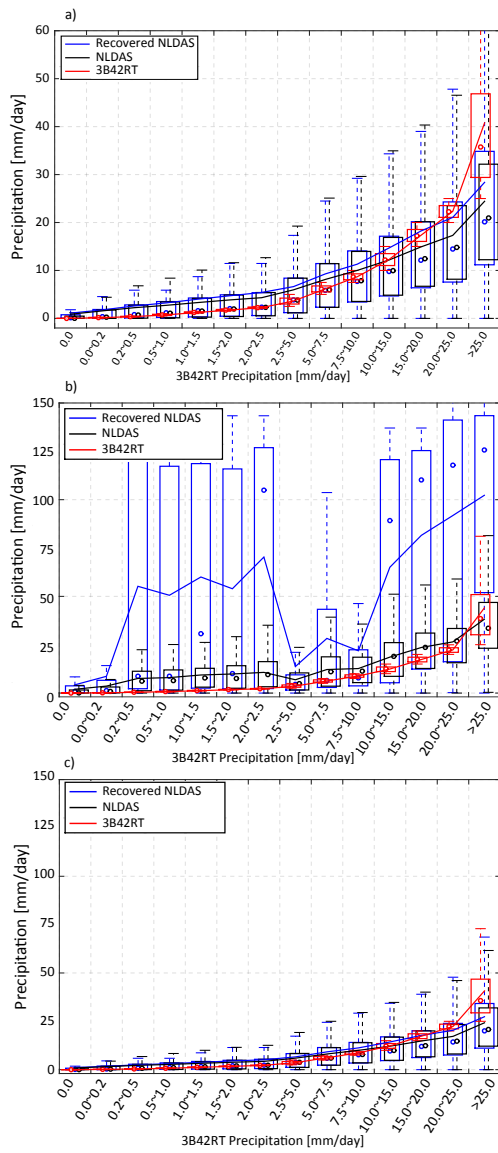
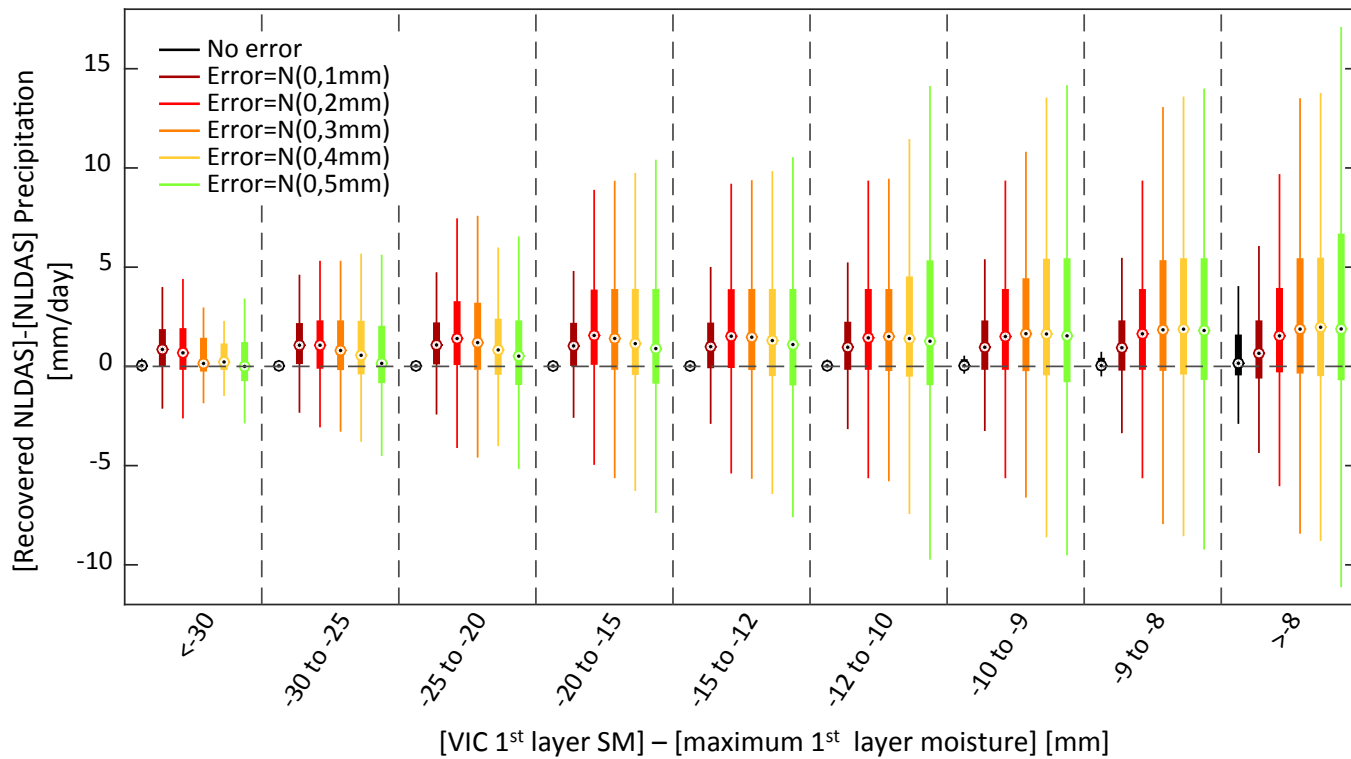


Figure 6 Accuracy of recovered precipitation in idealized experiment: (a) overall performance and separately comparing the improvement performance of recovered NLDAS precipitation (b) with and (c) without surface saturation condition. Statistics provided in Table 1.

Wang Zhan 9/7/2015 10:49 PM

Deleted: Table 1



1750

1751 Figure 7 Error in recovered NLDAS precipitation given surface moisture condition. Recovered NLDAS is based on using “truth” soil
 1752 moisture and soil moisture with normal error: $N(0,1\text{mm})$, $N(0,2\text{mm})$, $N(0,3\text{mm})$, $N(0,4\text{mm})$ and $N(0,5\text{mm})$. Statistics provided in

1753 [Table 2](#)

1754

Authors 8/31/2015 3:38 PM
 Deleted: .5mm

Authors 8/31/2015 3:38 PM
 Deleted: 1.0mm

Authors 8/31/2015 3:38 PM
 Deleted: 1.5mm), $N(0,2.0\text{mm})$, $N(0,2.5\text{mm})$,
 $N(0,3.0\text{mm})$, $N(0,3.5\text{mm})$, $N(0,4.0\text{mm})$,
 $N(0,4.5\text{mm})$

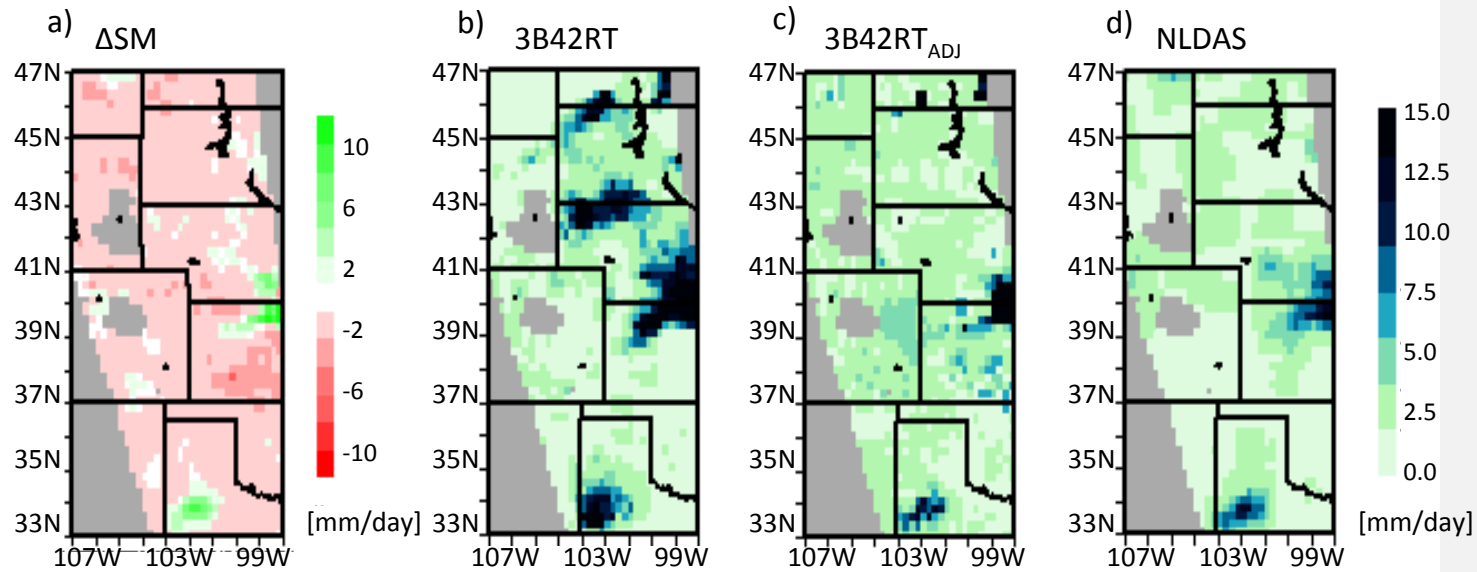
Authors 8/31/2015 3:38 PM
 Deleted: 5.0mm

Wang Zhan 9/7/2015 10:49 PM
 Deleted: Table 2

Authors 8/31/2015 3:38 PM
 Deleted: Page Break

a) ΔSM

b) 3B42

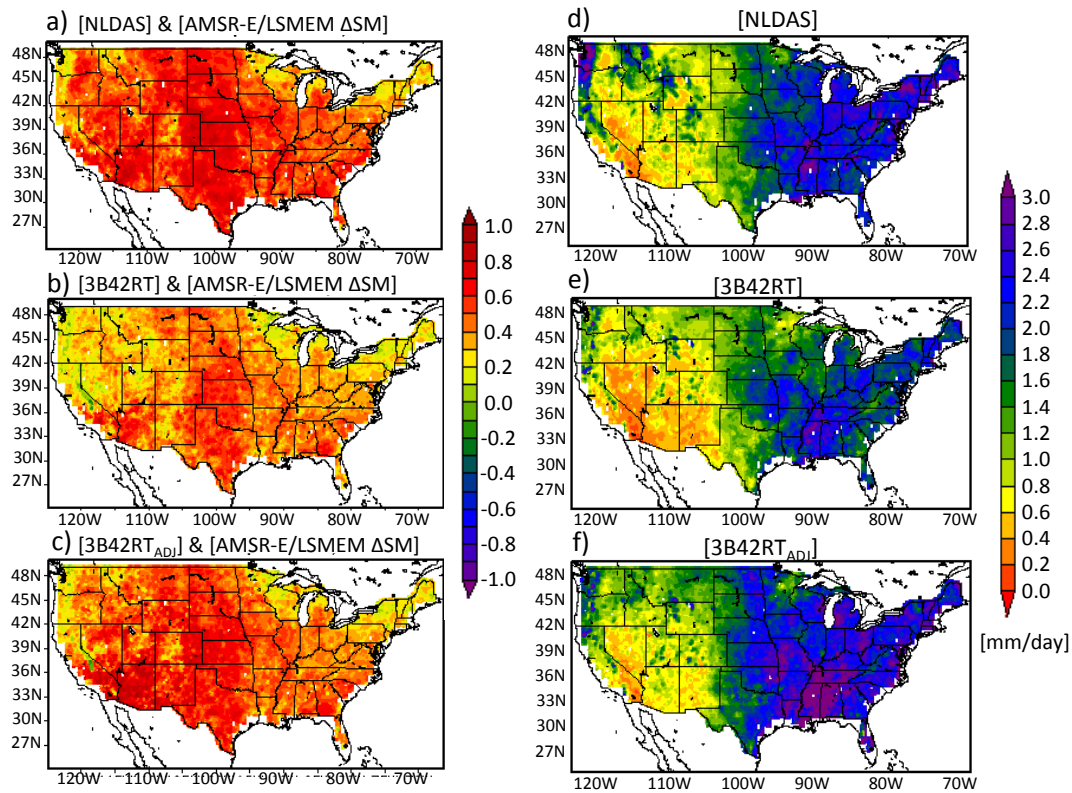


1764

1765 Figure 8 May 26th 2006 Rainfall pattern in 3B42RT (b) against NLDAS (d) as detected by AMSR-E/LSMEM Δ SM (a), and recovered
 1766 rainfall field (3B42RT_{ADJ}) by assimilating AMSR-E/LSMEM Δ SM (c). Gray shading shows area without soil moisture retrievals.

1767

Authors 8/31/2015 3:38 PM
 Deleted: into TMPA
 Authors 8/31/2015 3:38 PM
 Deleted: Page Break
 ... [349]



1772

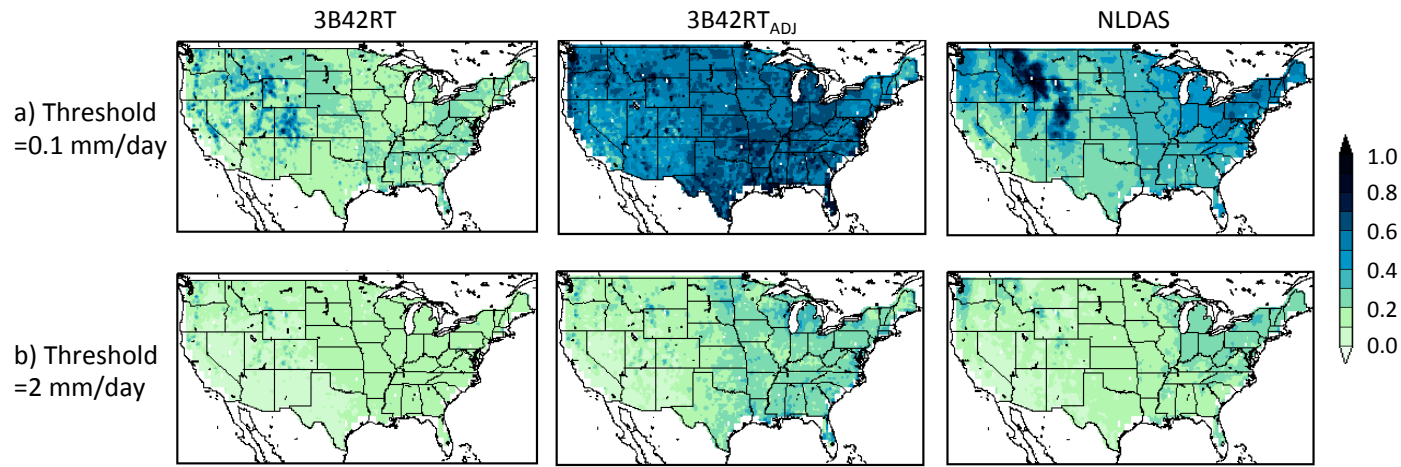
1773 Figure 9 Pearson correlation coefficient between AMSR-E/LSMEM Δ SM and precipitation: a) NLDAS, b) 3B42RT and c)
 1774 3B42RT_{ADJ}; annual mean precipitation in d) NLDAS, e) 3B42RT and f) 3B42RT_{ADJ} of time steps with AMSR-E/LSMEM Δ SM
 1775 retrievals.

Authors 8/31/2015 3:38 PM

Deleted: FAR, POD

Authors 8/31/2015 3:38 PM

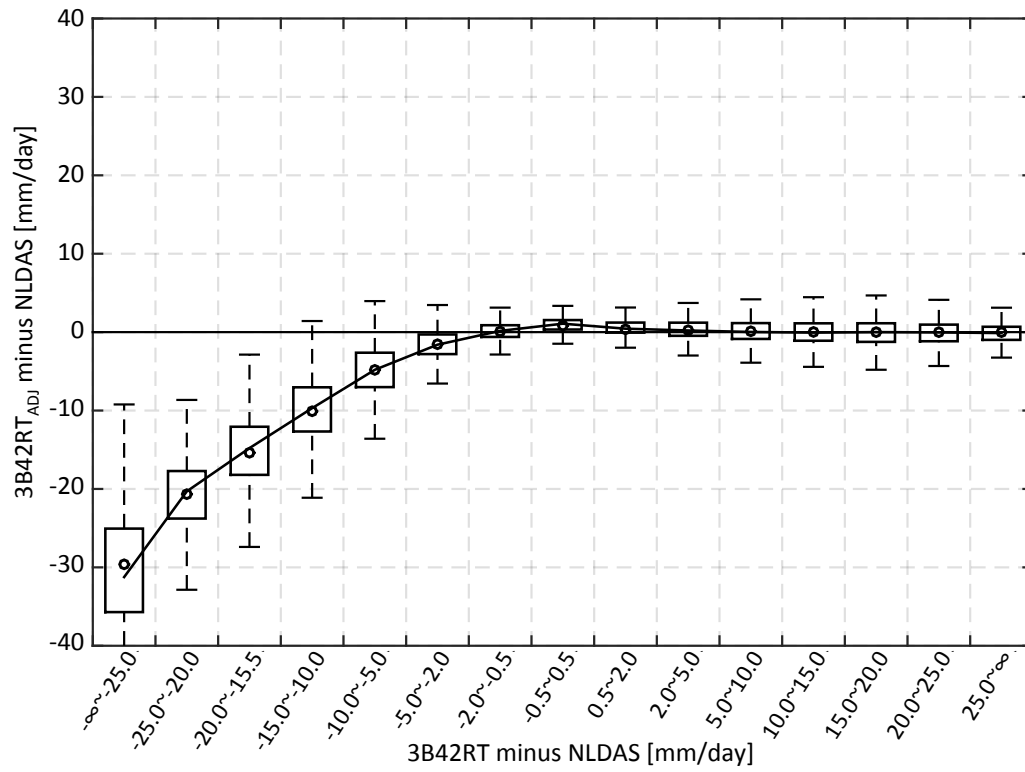
Deleted: frequency of rainy days



1778
1779
1780
1781

Figure 10 Frequency of rainy days in 3B42RT, 3B42RT_{ADJ} and NLDAS with a) 0.1 mm/day and b) 2 mm/day rainfall threshold to define a rain day.

- Authors 8/31/2015 3:38 PM
Deleted: 1mm
- Authors 8/31/2015 3:38 PM
Deleted: (top)
- Authors 8/31/2015 3:38 PM
Deleted: 2mm
- Authors 8/31/2015 3:38 PM
Deleted: (bottom)
- Authors 8/31/2015 3:38 PM
Deleted: event
- Authors 8/31/2015 3:38 PM
Deleted: [350]

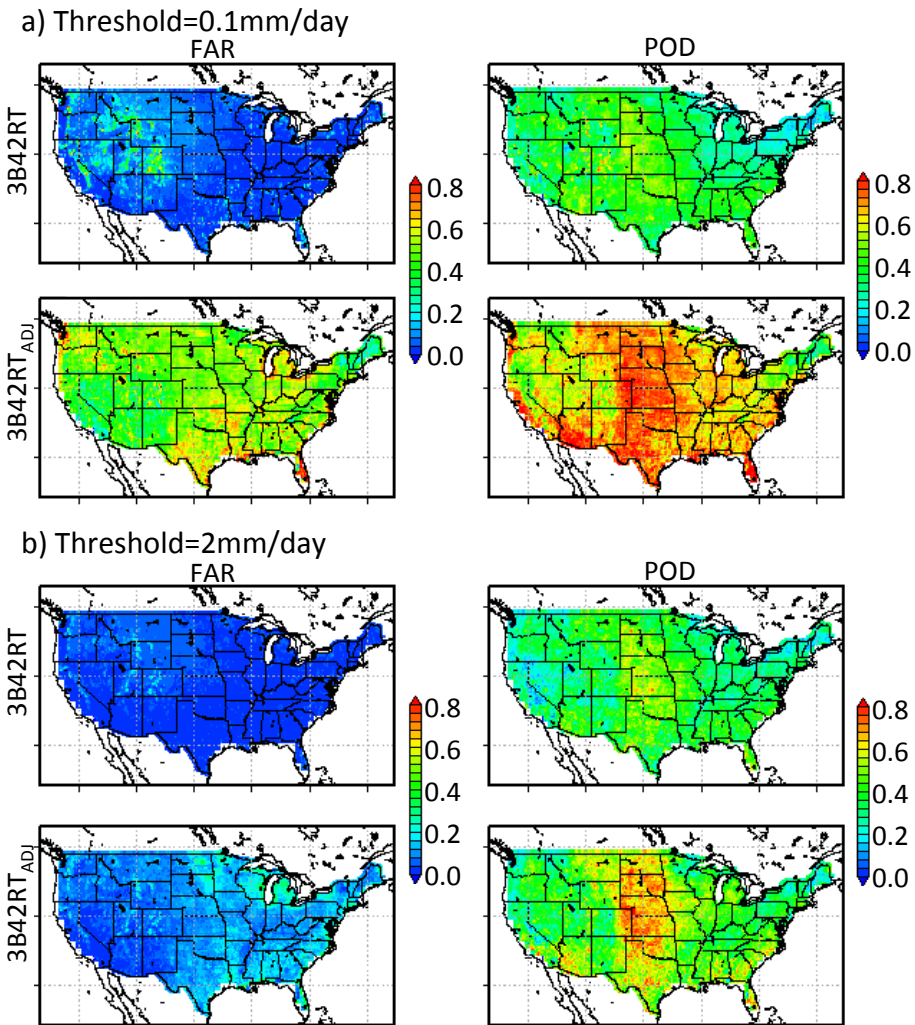


1789

1790 Figure 11 Distribution of 3B42RT and 3B42RT_{ADJ} precipitation error compared to NLDAS. Statistics are provided in [Table 3](#).

1791

Wang Zhan 9/7/2015 10:49 PM
 Deleted: Table 3
 Authors 8/31/2015 3:38 PM
 Deleted: Page Break
 ... [351]



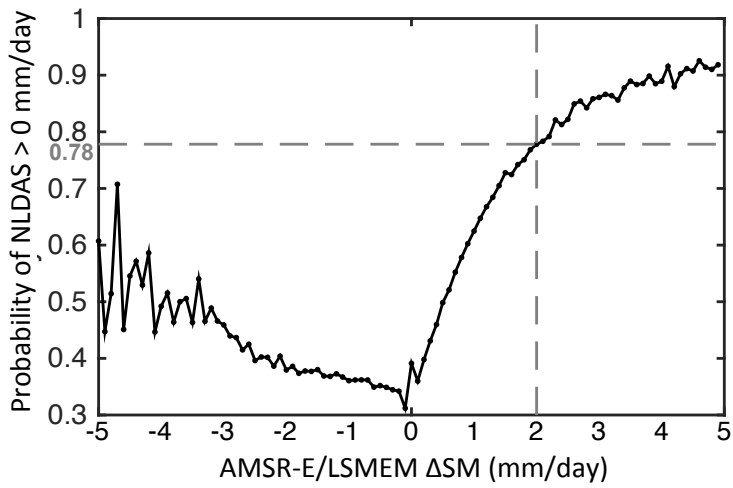
1796

1797

1798

Figure 12 FAR and POD of 3B42RT and 3B42RT_{ADJ} with a) 0.1 mm/day and b) 2 mm/day rainfall threshold to define a rain event.

- Authors 8/31/2015 3:38 PM
- Deleted:** (a-b) Difference in mean absolute error
- Authors 8/31/2015 3:38 PM
- Deleted:** and 3B42RT compared to NLDAS (MAE(3B42RT_{ADJ})-MAE(3B42RT)); (c-d) same as (a-b), after 2mm
- Authors 8/31/2015 3:38 PM
- Deleted:** cutoff ΔSM
- Authors 8/31/2015 3:38 PM
- Deleted:** is applied



1806

1807

1808

1809

Figure 13 Probability that the added rainy days ($3B42RT = 0$ mm/day, $3B42RT_{ADJ} > 0$ mm/day) are true rain events ($NLDAS > 0$ mm/day) given corresponding AMSR-E/LSMEM Δ SM.

Authors 8/31/2015 3:38 PM
 Deleted: Page Break
 ... [352]

Authors 8/31/2015 3:38 PM
 Deleted: Distribution of

Authors 8/31/2015 3:38 PM
 Deleted: when rainy days are added in $3B42RT_{ADJ}$ (no rain in $3B42RT$, rain in $3B42RT_{ADJ}$)

Authors 8/31/2015 3:38 PM
 Deleted: ... [353]